NONLINEAR FINITE ELEMENT MODELING AND ANALYSIS OF TIRE DEBRIS IMPACT ON AIRCRAFT STRUCTURAL COMPONENTS

A Thesis by

Dheeraj Chaitanya Thotakura

Bachelor of Engineering, Jawaharlal Nehru Technological University, 2012

Submitted to the Department of Mechanical Engineering
and the faculty of the Graduate School of
Wichita State University in partial fulfillment of
the requirements for the degree of
Master of Science

May 2015

NONLINEAR FINITE ELEMENT MODELING AND ANALYSIS OF TIRE DEBRIS IMPACT ON AIRCRAFT STRUCTURAL COMPONENTS

The following faculty members have examined the final copy of this thesis for form and content, and recommend that it be accepted in partial fulfillment of the requirement for the degree of Master of Science with a major in Mechanical Engineering.

_____
Dr. Hamid M. Lankarani, Committee Chair

_____
Dr. Rajeev Madhavannair, Committee Member

_____
Dr. Ehsan Salari, Committee Member

DEDICATION

To my Parents Ramalingeshwara Rao and Chiranjeevi Krupa Jyothi

ACKNOWLEDGMENTS

I would like to express my sincere gratitude and appreciation to my advisor, Dr. Hamid M Lankarani, Professor of Mechanical Engineering, for his valuable help, guidance and support. His constant encouragement and motivation helped me to complete my graduation studies at Wichita State University. I would also like to extend my gratitude to the members of my committee, Dr. Rajeev Madhavannair and Dr. Ehsan Salari for their valuable suggestions and helpful comments on my thesis.

I would like to thank Mr. Vikas Yadav, Engineering Specialist at Airbus Americas, for all the valuable advice, guidance and support he had provided me for the completion of my thesis. I want to thank all of my friends for their support. Finally I want to thank my parents who gave me moral support, encouragement at all stages of my education.

ABSTRACT

The aim of this research is to develop a methodology which can be utilized to certify an aircraft for tire debris impact onto structural components and also to predict structural response by numerical simulation. After the aircraft experiences a tire burst scenario, tire debris projected from the rotating tire can impact the structural components of the aircraft. European Aviation Safety Agency's notice of proposed amendments (CS 25.734) demonstrated that the structural components and systems which are essential to the safe operation of aircraft should be protected from the damaging effects of tire debris.

In this study, a computational methodology is developed to model and analyze the effects of tire debris impact on aircraft structural components. Experimental data from the tire fragment impact test on to the aluminum plate is compared with the numerical data to validate the tire debris model developed in this study. Parametric study is then conducted on validated tire debris model by impacting it onto the aircraft inboard flap. Inboard flaps are one of the major structural parts which are located in the zone of vulnerability defined by European Aviation Safety Agency and Federal Aviation Administration. Structural deformations and energy analysis on inboard flap by impacting tire debris model at two locations for different angle of attack and varying impact velocities are to be considered for this study.

Detailed geometry of the inboard flap for the aircraft and tire debris are modeled in Catia V5 R21. Finite element modeling and fastener connections are defined in Altair Hypermesh 12.0. Material properties and boundary conditions are defined in LS-Prepost 4.2. This study provides a computational methodology to certify aircraft as per certification standards. This methodology provides design engineers the effects of tire debris impact on a structural component and also to change initial design requirements for structural components.

TABLE OF CONTENTS

LIST OF TABLES

LIST OF FIGURES

LIST OF FIGURES (continued)

Figure Page

LIST OF FIGURES (continued)

Figure Page

LIST OF ABBREVIATIONS

FAA	Federal Aviation Administration
EASA	European Aviation Safety Agency
CS	Certification Standards
AC	Advisory Circular
DOE	Design of Experiment
FEM	Finite Element Mesh
RCC	Reinforced Carbon Carbon
NASA	National Aeronautics and Space Administration
CAD	Computer Aided Design
KE	Kinetic Energy
IE	Internal Energy

CHAPTER 1

INTRODUCTION

1.1 Background

There will always be a probability of tire burst incident occurring for an aircraft during takeoff or on landing. Federal aviation records demonstrate that the major cause for tire burst scenario is through foreign object debris on the runway [10]. Some of the common causes for tire failure are the strains suffered by tire due to centrifugal force. Under inflation or over inflation of the aircraft tire may also lead to tire burst. Another factors for tire burst is landing of the aircraft with more weight than recommended and also high taxi speed of the aircraft with more than maximum takeoff weight. Tread wear is also the major cause for tire burst. As per FAA regulation when tire failure is detected for an aircraft, takeoff for that aircraft should be rejected prior speeds reaching up to 80 knots. If the aircraft crosses 80 knots, it should continue to its destination unless there is damage occurred to engine or other systems which are vital for aircraft's safe flight. Maintenance of the tire also plays an important role for the tire failure. Regular check for tire pressure and thorough inspection of tire would reduce the tire failure to some extent. Tire debris generated from tire burst when impacted onto the aircraft's structures and systems may sometimes leads to catastrophic failure conditions. Various accidents were reported in recent years which resulted in catastrophic failure of the structural parts beyond repair.

The catastrophic accident occurred to Concorde flight 4590 on 25 July 2000 in France was caused by tire debris impact onto underside of left wing [1]. Tire debris impacted on to the underside of the wing created pressure surge by rupturing the fuel tank and initiating fire which

resulted in engine failure and damage to the aircraft. Boeing 747-122 flight number N4714U on 16th November 1984 has aborted take-off after the main landing gear tire has blown out causing tire debris to penetrate into fuel tank access panel under the right wing [3]. There were reported cases of multiple tire debris being impacting on the underside of aircraft in a single tire burst event causing structural failure of the components.

Figure 1.1 Damage due to tire burst and tire debris impact on inboard structural components [2].

Tire burst incident for Bombardier global express BD700 on 9th December 2005 in Taiwan caused system failure and structural component failure in the aircraft [2]. Just after the aircraft landed on the runway it experienced tire burst with failing tire debris impacting under part of the wing left wing causing structural damage to hydraulic systems with a broken inboard substructure of the left wing. As shown in figure 1.1, Inboard flap has also experienced structural damage along with electrical wires on left main landing gear.

1.2 Certification Standards

In order to assess the above mentioned situation and other similar incidents, Federal Aviation Administration (FAA) and European Aviation Safety Agency (EASA) have come up with the following requirement standards for certifying the aircraft against damage caused by tire and wheels failures on the aircraft as mentioned in table 1.1.

TABLE 1.1

CERTIFICATION STANDARDS

FAA Advisory Circular 25.729 (f)	Protection of equipment on landing gear and in wheel wells [9]
FAA Advisory Circular 25.963	Fuel tank access covers [7]
FAA Advisory Circular 25.1309-1A	System design and analysis [8]
EASA CS 25.734	Protection against wheel and tire failure [10]

European Aviation Safety Agency has proposed new certification standards through CS 25.734 which requires aircraft to fly safely and also components should be in safe operation in the event of a tire failure. One of the revised methods from CS 25.734 for aircraft with gear extended case is modeling tire debris for impact analysis on structural components [10]. EASA and FAA define the zone of vulnerability to be the zone where there is probability of tire debris impacting the aircraft. As shown in figure 1.2, FAA and EASA have defined the zone of vulnerability in the range of 135^{o} arc when seen from the side view of the tire. The zone of vulnerability starts from plane which is 45^{0} to the ground horizontal plane from rearward direction and ends in the plane which is 180^{0} to the ground horizontal plane from the forward direction.

There would be probability of high energy impact when tire debris is released from the tire in this zone. When seen from the front view of the tire, zone of vulnerability is defined at an angel Θ^{0} from the plane perpendicular to the ground horizontal plane. Angle Θ is defined as 15^{0} for large tire debris model and 30^{0} for the small debris model.

As per the certification standards, threat occurs to the aircraft when tire debris is released from the tire which is rolling on the ground.

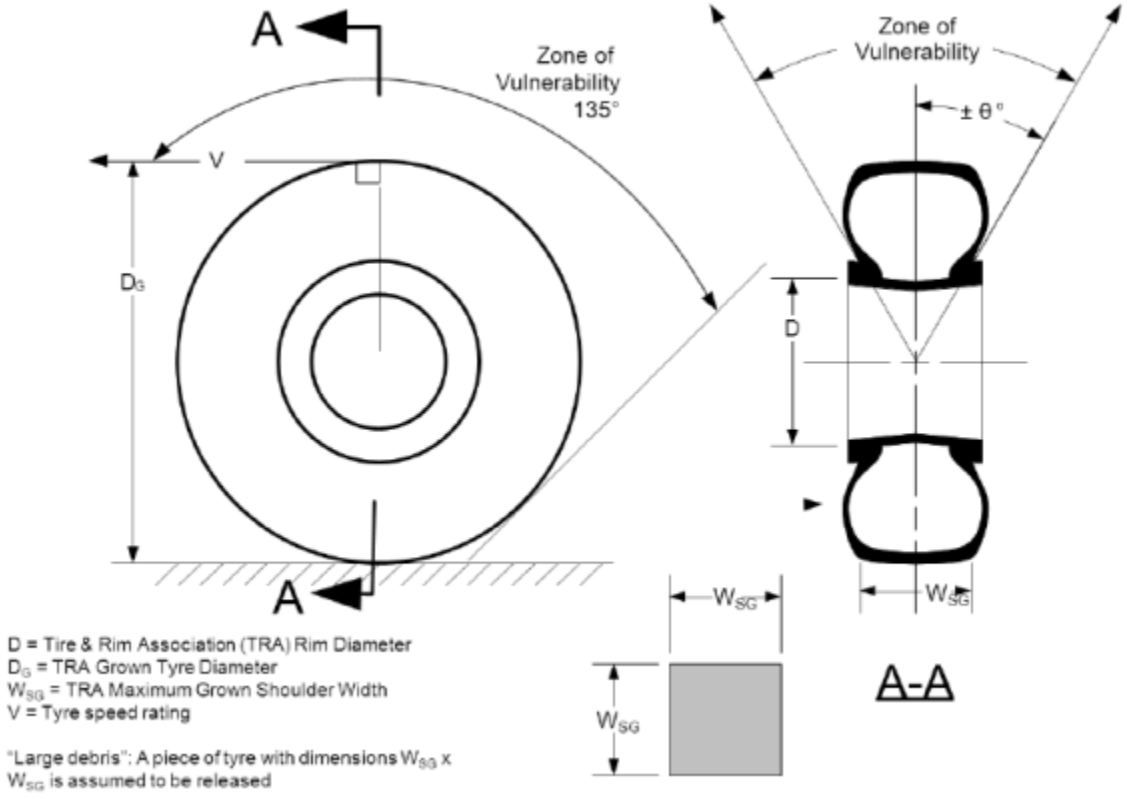

Figure 1.2 Zone of vulnerability defined for tire debris impact model [10].

There are two tire debris sizes to be considered for certification. Large tire debris will have dimensions W_{SG} X W_{SG} , where W_{SG} is the maximum grown shoulder width of the tire and the thickness of the tire debris is defiend as the total width of tread plus outermost reinforcement ply from the new tire [10]. Small debris model is defined to have 1% of the total tire mass with distribution of impact load over an area which is 1.5 times the area of the tire tread as shown in figure 1.3. CS 25.734-4(3) states that two debris sizes should be considered for protection of systems from tire debris impact with pass-fail criteria. But when there is requirement for protection of structural components or system or for validation of structural parts of the system,

small debris size should be used.

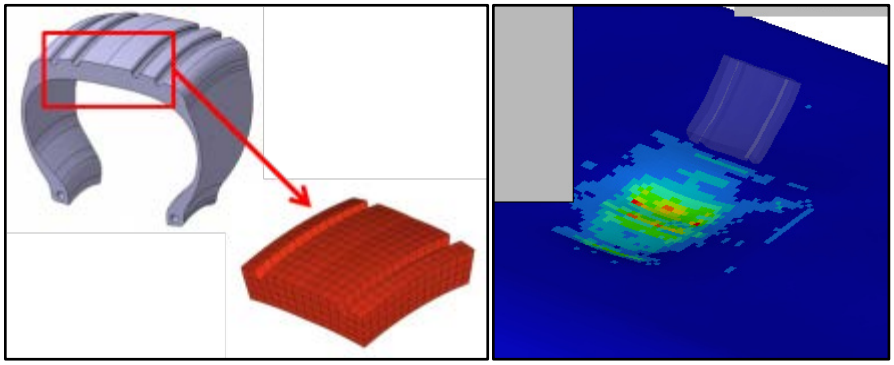

Figure 1.3 Requirements for small debris model as defined in CS 25.734 [10].

1.3 Motivation

In the event of a tire burst for an aircraft, there will always be a chance of tire debris being impacted onto the aircraft. This can happen during takeoff or on landing of the aircraft. Tire debris can cause severe damage to the structural components of the aircraft if it impacts at high velocity. Any damage to the vital components can result in nonfunctioning of the aircraft, which can be threat to human lives. There will always be a risk of fire accident if the tire debris penetrates into the fuel tank. It is always necessary to certify the aircraft's structural components in order to prevent catastrophic failure. Experimental testing of the structural parts would be a time taking and expensive process. When compared to experimental tests, numerical simulation can be repeated number of times and also plays an important role during design optimization of the structural components. There can be an efficient way to certify the aircraft structural components by finite element analysis tools. A methodology is proposed in this research to do the process of certification by analysis for tire debris impact.

CHAPTER 2

LITERATURE REVIEW

Ryabov [13] performed simulations on deformation of landing gear compartment wall under air jet loading and impact of tire piece on the pipeline for Sukhoi superjet-100. A detailed computer simulation was performed for validation. The elastic plastic deformation of the steel pipe was calculated by impacting tire piece with a speed of 120 m/s. Tire piece model is composed of solid elements with an average size of 5mm and average weight of 1kg. Simulation of plate deformation was performed in LS-Dyna and results are compared with experimental data. This source has information on material properties to be used for tire fragment model.

Boesch [14] focused on detail modeling of automobile tires for crash applications. He focused on developing more detailed tire model which is computationally cost effective for usage in impact simulations. Different types of rubbers are used in tires, some of them which provide lower stiffness for more flexibility and some with higher stiffness for durability. The tire model was comprised of five different sections, where the tire's tread was modeled with fully integrated solid elements. Side wall which provides the lateral stability to the tire was modeled with fully integrated shell elements to reduce hourglass effects. The steel beads which carry force from the sidewall are modeled using beam elements. Steel belts between tread are modeled with beam elements and body plies which run perpendicular to the steel belts are also modeled with beam elements. Simulation was performed for the modeled tire in compression mode and was compared to laboratory testing. Simulating the new model of tire for impact simulations exhibits a near relation with the testing data.

Barbani [15] worked on finite element simulations on motorcycle tire behavior during crash. It requires more detail modeling of motor cycle tire during crash scenario because of the different layouts of vehicle structure. Author modeled two different types of mesh for tread and sidewall, one being shell mesh and other a solid mesh. Mooney Rivlin material model was used as material for tread and sidewall rubber. Experimental results were carried out by compressing the tire to a steel plate which acts as a rigid wall. This simulation uses Design of Experiment (DOE) analysis to calculate the parameters influencing the behavior of the model. After the simulation, it was proved that the two models have provided accurate results and the model with shell elements took less time to compute than the solid elements.

Orengo [16] developed a methodology to model pneumatic tire to use it in impact simulations. The tire model which is modeled with shell elements and having uniform thickness is computationally stable but also leads to unrealistic tire behavior when it undergoes large deformations. The tire model is behaved linearly under small loads. As the load is increased gradually, the deformations of the tire model increases and the shell surface converse itself into the tire. As elements in LS-Dyna do not have out of plane bending stiffness, deformation associated with the elements will cause numerical instability. A refined mesh is required to overcome the tangled or deformed elements. Shell elements are used to model the bead coils. Radial reinforcement in tire is modeled as beam elements with Belytschko-Schwer element formulation. Side walls are modeled as shell elements with Belytschko-Tsay element formulation. Computational stability is achieved as the tread of the tire is modeled with under integrated hexahedral elements to avoid hourglass modes with no effect on time step. The completed model was numerically simulated with compression test and guardrail impact test.

Konde [17] studied on generating a detailed 3D tire model for finite element analysis.

Rubber was modeled using Mooney Rivlin hyperelastic material and the reinforced fibers are modeled with linear orthotropic elastic model. Tension test was performed for the tire samples and the material properties are derived for simulation. The model was created by using 3d solid elements. Before creating the solid elements, the author used shell elements for the mesh of cross-section of tire and then rotated the mesh with equal intervals for creating a solid mesh. By using this modeling technique, it would be easier to maintain the element size along the cross-section of the tire.

Shang [18] dealt with the impact testing of wheel. Where the main purpose is to enhance the mechanical performance of wheel and also lower its development cost by executing numerical simulations. In order to simulate the dynamic impact performance of the wheel, author used nonlinear material model. Author chose LS-DYNA as explicit FEM code for numerical analysis of tire impact. The tire model was divided into carcass and tread for simplification. Tire carcass was modeled using single layer of shell elements. Tread was modeled using solid elements. Mooney Rivlin material card (*MAT_27) was used for the tire model. True stress and true strain values were required as an input values for the simulation. They were calculated from engineering stress and engineering strain values obtained from testing.

Blundell [19] constructed a detail finite element tire model to investigate the tire performance and its safety assessment. As the detail finite element model was considered; tread, sidewall, apex, and bead are modeled with solid elements. Plies and belts are modeled with beam elements and shell elements. Initially 2D model with shell elements were created with minimum element size around 5mm. 3D tire model was attained by rotating the shell elements in 2D cross-section along 360 degrees with equal intervals to obtain solid elements. Beam

elements for the plies and beads were generated from solid elements. Material model for the tread was chosen as hyperelastic rubber from LS-Dyna. FE model of the tread was validated by comparing simulation values to experimental values.

Yang [20] adopted ABAQUS for developing detailed finite element model of the tire and also to capture details of tire tread reinforcements. Tire is categorized into tread, under tread, apex, sidewall and inner liner along with reinforcements for detailed finite element analysis. Finite element model comprised of 2D shell elements which were meshed along the cross section of the tire, later they are rotated along axisymmetric axis to attain 3D solid elements. Different material properties are considered for tread and sidewall due to different proportions of rubber used. As the rubber exhibits high nonlinear stress strain behavior, tread and plies are modeled with high modulus viscoelastic material.

Mines [21, 23 & 24] and others had investigated on simulation approach for tire debris impact on the fuel tank access panels. In order to obtain material properties of tire debris, quasi-static tests have been conducted on the test specimens. Cylindrical specimen consisting of reinforced core along tread material was taken for compression test with diameter 25 mm as its behavior would be stable under compression. Impact tests are conducted with velocities ranging from 50 m/s to 135 m/s to measure strain rate of the material. For impact test of tire specimen onto access panel, the velocity with which fragment was impacted is around 135 m/s. Strain gauges were attached to the panel to measure its structural response. The finite element model for the tire specimen has solid elements and beam elements as reinforcement layers connecting nodes. In order to define material properties for the tire, Mooney Rivlin material model is considered as material card. Wing access panel is modeled with solid and shell elements and screws are modeled as tied contact which is fixed to the surface of access panel. Contact

formulations are defined between tire and panel before impact analysis is conducted.

Lyle [22] developed probabilistic analysis to determine the effects of debris impact on composite panels using LS Dyna. Lyle performed structural impact analysis on reinforced carbon-carbon RCC panels to improve NASA space shuttle program. Lyle simulated debris impact on the shuttle's thermal protection system and validated the model by comparing experimental and numerical results. Factors like impact conditions, material properties and fabrication defects play a crucial role in impact analysis. Before analyzing the impact on leading edge panel, impact test on reinforced carbon-carbon panel with foam is performed to validate the model and its material properties. Cylindrical foam is impacted with velocity ranging from 397 to 695 ft/s on to RCC panel with 1.5X6 inch in dimension. Finite element model is developed to run computationally efficient and also to ensnare physics of the structural impact. Composite panel is modeled with MAT # 58 and foam is modeled with MAT # 83 in Ls Dyna. Probabilistic analysis is performed to measure the response of leading edge panel to debris impact.

After an examination of the literature review, it was observed that there was lot of research on finite element modeling of rubber models, and also process and techniques required for impact test through numerical simulations. It is decided to use the modeling method defined from sources, Boesch [14] and Barbani [15], to define finite element model for tire debris. Material card for tire debris model which is assigned in LS Dyna used for this thesis is defined from sources, Konde [17] Shang [18]. Experimental data for validation of the tire debris model is used from the references [21, 23 and 24].

CHAPTER 3

METHODOLOGY

3.1 Objective

The objective of this research is to develop a methodology which can be utilized to certify an aircraft for tire debris impact onto structural components and also to predict structural response by numerical simulation. Methodology for the tire debris impact analysis for this thesis is shown in figure 3.1.

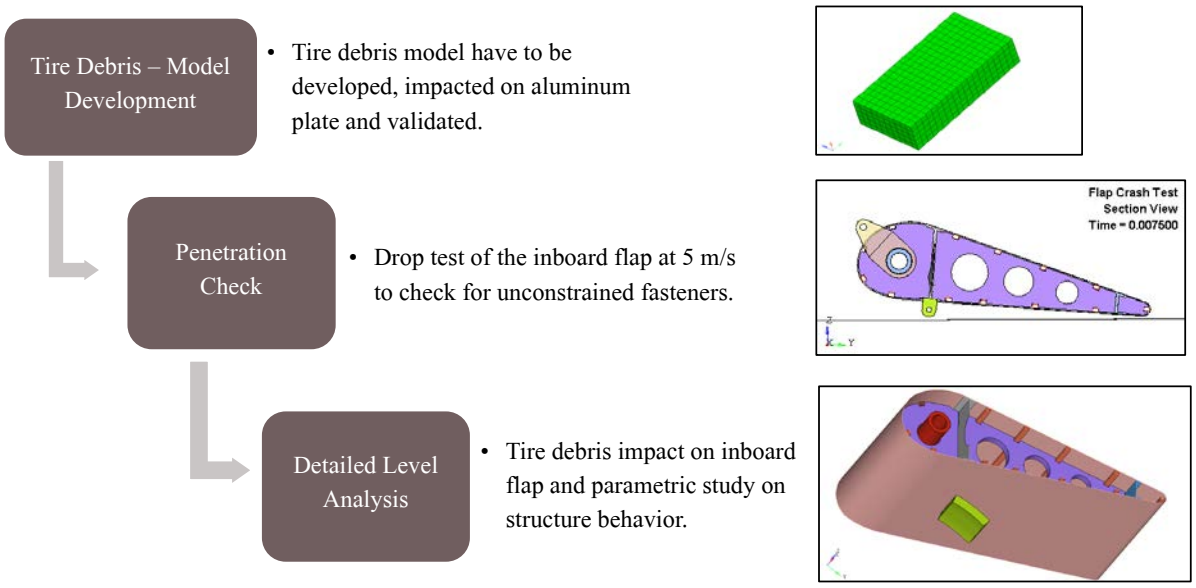

Figure 3.1 Methodology for tire debris impact analysis.

3.2 Methodology

In order to validate the methodology, numerical model of the tire debris have to be validated by comparing numerical simulations which are carried out using non-linear finite element analysis solver LS-Dyna with the experimental test results from reference [23].

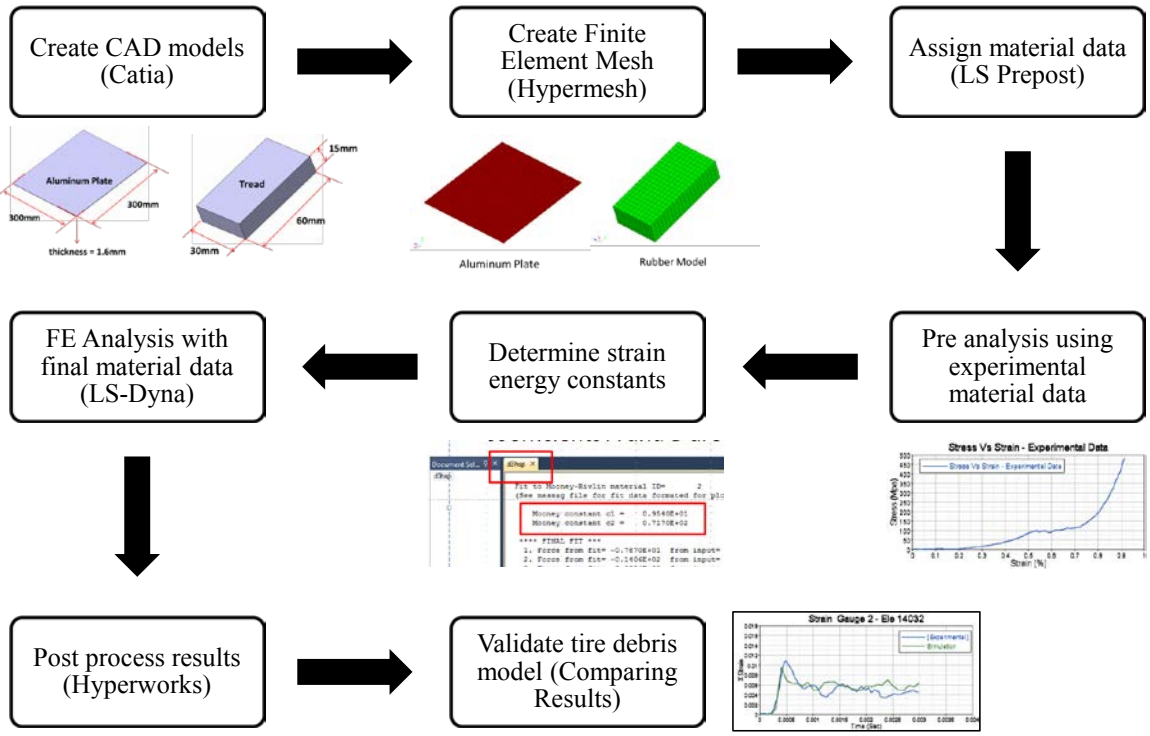

Figure 3.2 Methodology for tire debris model development.

Methodology for validating the tire debris model is shown in the figure 3.2. All the required models are designed in Catia V5 R21. Finite element mesh is created using Altair Hypermesh 12.0. All the material properties are taken from the reference [23]. Material cards are created in LS Prepost 4.0. Pre analysis is simulated in LS Dyna by inputting experimental material data for rubber model and calculating strain energy constants. Post analysis is performed with revised material properties for rubber model. Strains at impact locations are calculated from strain gauges located on aluminum plate from experimental test are compared with numerical simulation data in order to validate the tire debris model.

Parametric study is then conducted by impacting validated tire debris model on to the aircraft inboard flap as shown in figure 3.3.

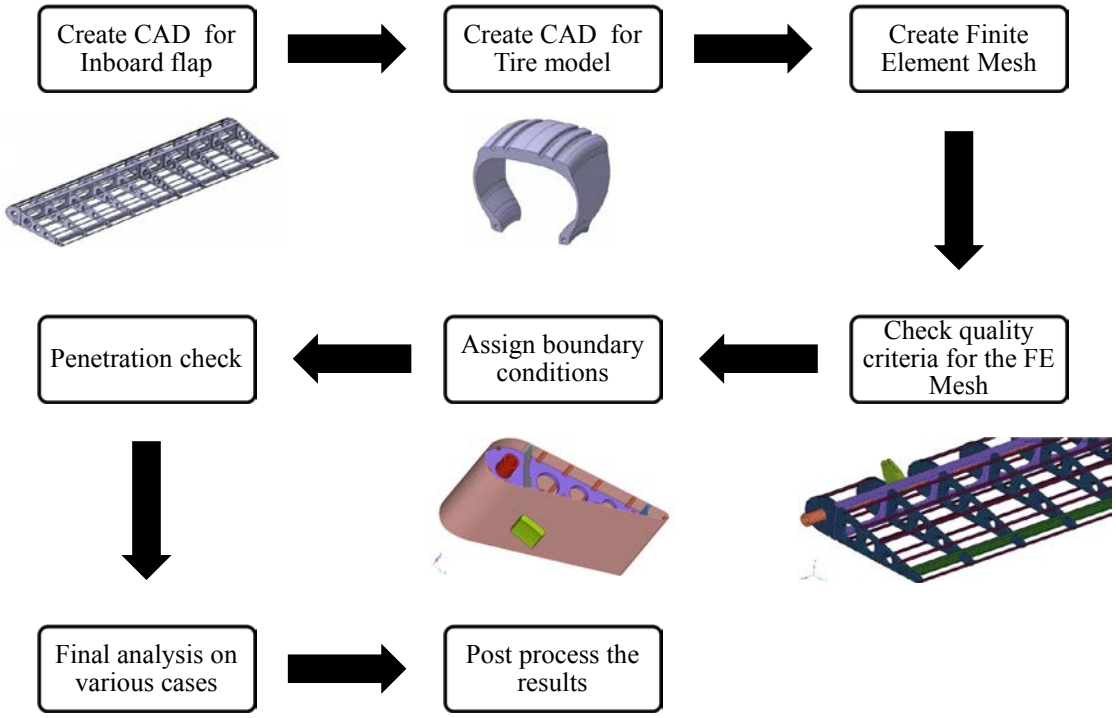

Figure 3.3 Methodology for parametric study of flap impact analysis.

European Aviation Safety Agency and Federal Aviation Administration standards define that the tire debris can be impacted to any structural part which lies in the zone of vulnerability [10]. Aircraft inboard flap is one of the major structural parts which are located in this zone of vulnerability as shown in figures 3.4 and 3.5.

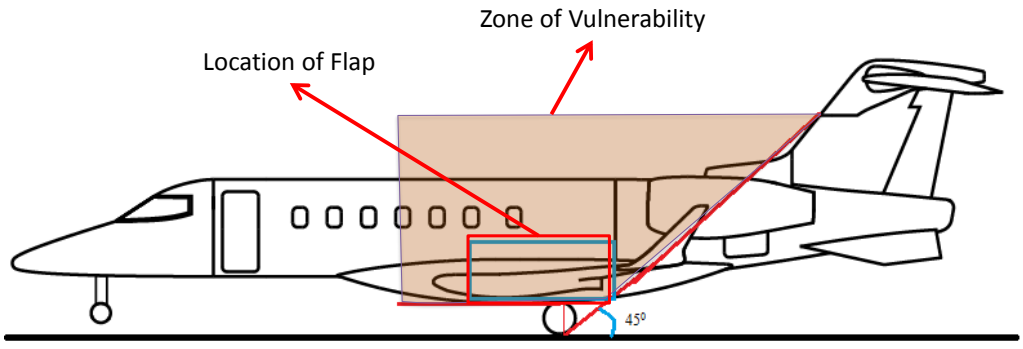

Figure 3.4 Location of flap on an aircraft, as seen from side [27].

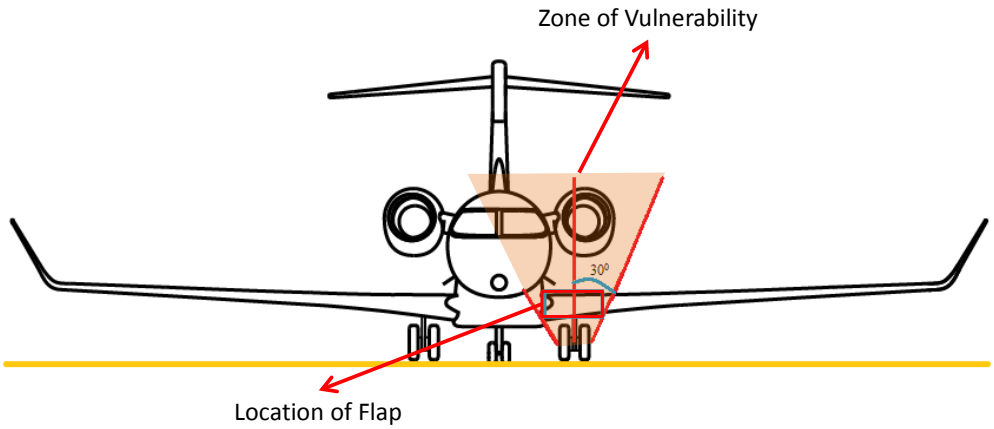

Figure 3.5 Location of flap on an aircraft, as seen from front [27].

Detailed geometry of the inboard flap of the aircraft is modeled from the reference [4, 5]. Detailed geometry of the aircraft tire is modeled from the reference [26]. Catia V5 R21 is used to model the geometries of tire and inboard flap. Finite element mesh is created for all of the components and is checked for the quality criteria. Fastener connections are defined for the components by using Altair Hypermesh 12.0. Material properties and boundary conditions are assigned of the components using LS-Prepost 4.2.

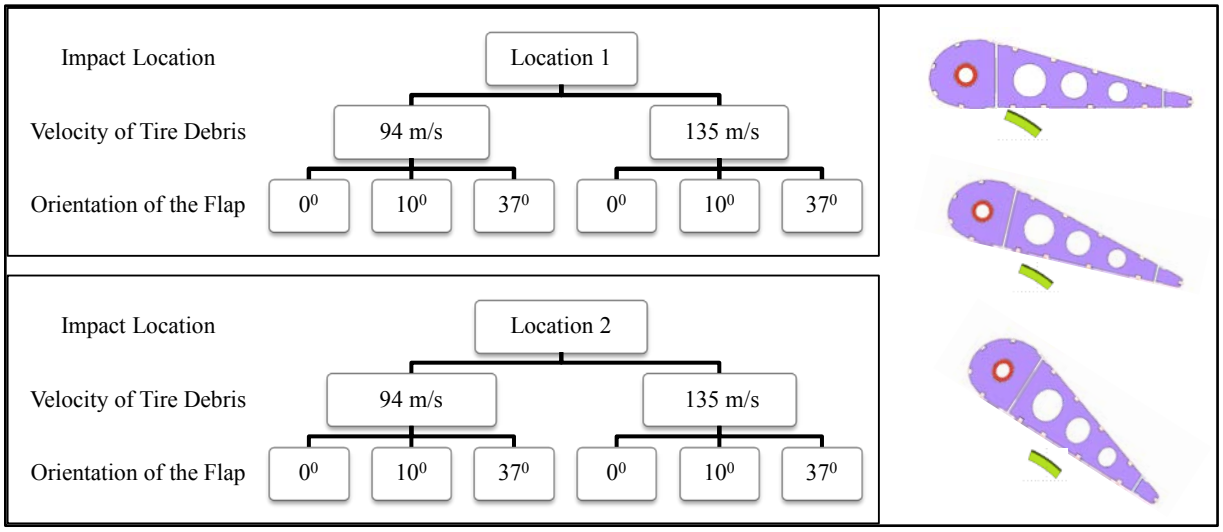

Figure 3.6 Methodology for parametric study

Figure 3.6 shows the methodology for parametric study. Two different velocities are considered in the study for impacting tire debris onto the inboard flap structure. Maximum tire speed rating recommended by tire manufacturer which is 94 meters per second and a fail safety velocity of 135 meters per second is also considered for this study [23]. Two impact locations are considered on the inboard flap which is in the area prone to be hit by the tire debris during landing or on takeoff. First impact location is in the forward section of the flap and the second location is towards the rearward section of the flap. As the flaps play a vital role during takeoff and after landing, flaps are oriented at three different angles for tire debris impact analysis. Flap oriented at 0^0 to the horizontal ground plane will be the normal case without lift and drag. Flap oriented at 10^0 to the horizontal ground plane would be high lift case which plays important role during takeoff. Flap oriented at 37^0 to the horizontal ground plane would be the high drag case which plays important role during landing [11].

Deformations of the structural components inside the inboard flap are observed for various impact cases and are tabulated according to severity of their damage. Energy analysis is performed on inboard flap by impacting tire debris model at two locations for different orientation of the flaps. Fasteners forces are also calculated and compared for failure analysis.

This study provides methodology to certify aircraft as per certification standards. This methodology can provide design engineers the effects of tire debris impact on a structural component which can help to change initial design requirements for structural components.

CHAPTER 4

DEVELOPMENT OF TIRE DEBRIS MODEL

The tire debris model has to be developed before it can be used for parametric study. Numerical simulation of tire debris model impacting on to the aluminum plate is compared with experimental test results to validate the tire debris model. Dimensions of tire debris model and the test configuration are obtained from literature [23].

Models of the CAD for impact test are created in Catia V5 R21 using the dimensions of the models from experimental test.

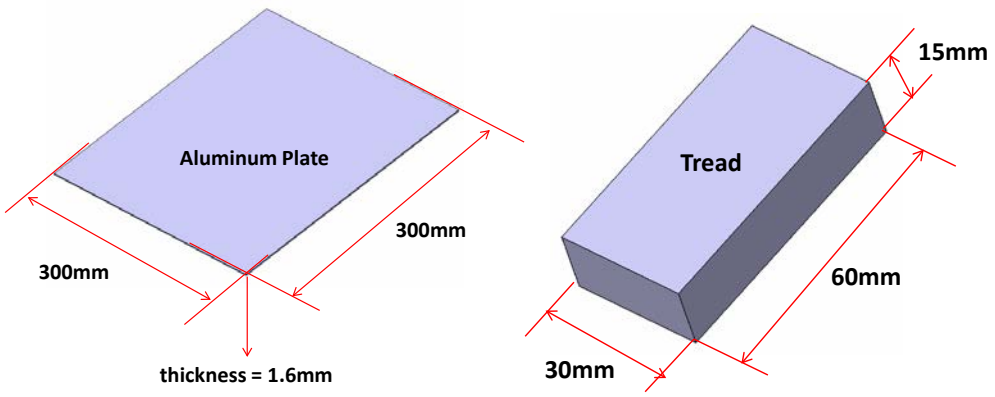

Figure 4.1 Geometry for tire debris model development [23].

Figure 4.1 shows the required models for aluminum plate impact test. Tire debris model used in this validation test is taken from a used Michelin aircraft tire and the aluminum plate used has similar configuration with the ones which are used in aircrafts. Aluminum plate used for impact test has the length of 300 mm, breadth of 300 mm and thickness of 1.6 mm. Tire debris model has the length of 60 mm, breadth of 30 mm and thickness of 15 mm. There were few tests performed by impacting tire debris model on to the aluminum plate which is

oriented at different angles. Test configuration of rubber model impacting aluminum plate oriented at 30^0 to the ground horizontal is selected for validation of the tire debris model.

4.1 Finite Element Models for Validation

Finite element mesh is generated from the CAD geometry of the models using Altair Hypermesh. Aluminum plate is meshed with shell elements as the thickness of the plate is 1.6 mm. Tire debris model is meshed with solid elements as the thickness of the tire debris model is 15 mm.

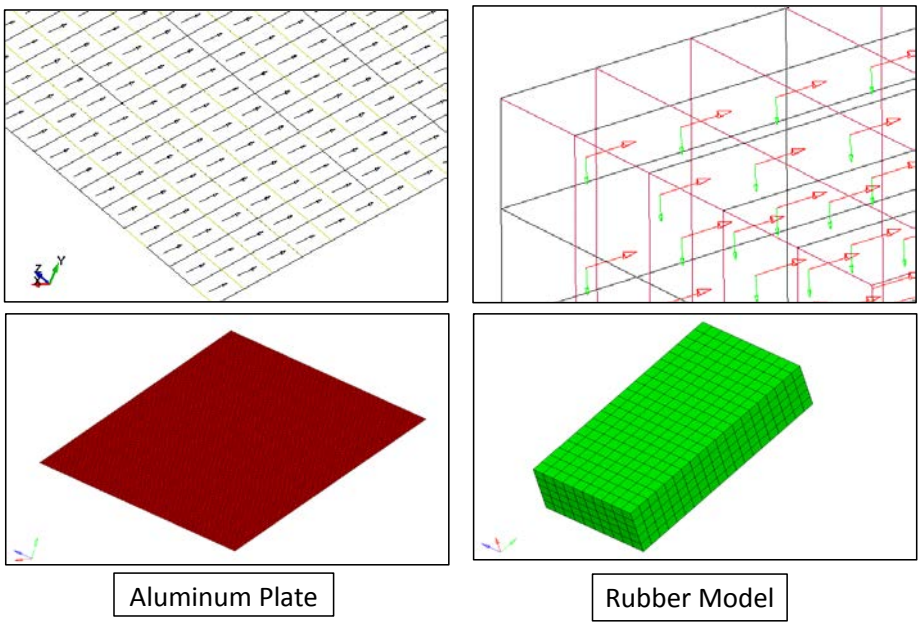

Figure 4.2 Element direction and finite element mesh for the tire debris model.

Elements are chosen to be modeled as shell mesh with minimum element size of 3 mm and a total of 10,000 elements for the aluminum plate [25]. Tire debris model impacting the aluminum plate is modeled as solid mesh with minimum element size of 3 mm and total of 1,000 elements [19]. Figure 4.2 shows the mesh for the models and element orientation for the finite element mesh. Material type of the plate is chosen as Aluminum 2024 T3 from the

reference [23]. *MAT_24 card (MAT_PIECEWISE_LINEAR_PLASTICITY) is chosen for assigning material properties to the plate in Ls Prepost. Material properties for the plate are shown in table 4.1 below. Thickness of the aluminum plate is defined using SECTION_SHELL card in Ls Prepost. Accurate results of stresses and strains have to be captured in the finite element mesh as the simulation is performed using nonlinear explicit method. Element orientation for the finite element mesh should be in uniform direction in order to capture accurate strain results in LS Dyna.

TABLE 4.1

MATERIAL DATA FOR AL 2024 – T3 [28]

Physical Property	**Metric**	**Units**
Density	2.768E-09	ton / mm^3
Modulus of Elasticity	72394.97	MPa
Poisson's Ratio	0.33	-
Yield Tensile Strength	332	MPa
Tangent Modulus	1341	MPa

Material Properties for the tire debris model is assigned using *MAT cards in Ls Prepost. MAT_MOONEYRIVLIN_RUBBER, which is *MAT_027 card in LS Dyna is chosen for the tire debris material [24]. For the tire debris model to behave hyper elastic, Mooney Rivlin constants have to be assigned for the model. Strain energy density function for the rubber material is defined in equation 4.1. Stiffness of the rubber material depends on the strain energy equations constants A and B, they are also known as Mooney Rivlin material constants.

$$W = A\,(I - 3) + B\,(II - 3) + C\,(III^{-2} - 1) + D\,(III - 1)^2 \qquad (4.1)$$

Where,

$C = 0.5\,A + B$

$D = \frac{A(5v-2)+B(11v-5)}{2(1-2v)}$

v = Poisson's ratio

$2(A + B)$ = shear modulus of linear elasticity

I, II, III = invariants of right Cauchy-Green Tensor C.

Pretest simulation is performed for tire debris model by assigning mass density and Poisson's ratio of the rubber in *MAT_27 card. Engineering stress vs engineering strain curve is inserted in the material card for the pretest simulation. As the experimental compression test data is available, stress vs strain curve must be inserted in negative y and negative x axis.

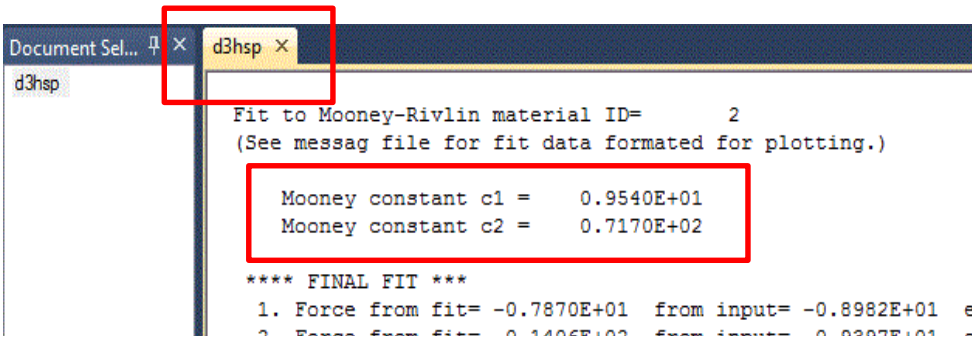

Figure 4.3 Mooney Rivlin constants generated in output file.

Mooney constants A and B are calculated and printed out in the output file which can be seen in figure 4.3. Mooney Rivlin constants A and B generated from d3hsp file are assigned to the rubber model in the material card for final simulation. Material properties for the rubber model are shown in table 4.2.

TABLE 4.2

MATERIAL DATA FOR TIRE DEBRIS MODEL [23]

Physical Property	**Metric**	**Units**
Density	1.020E-09	ton / mm^3
Poisson's Ratio	0.495	-
Mooney Constant A	9.54	-
Mooney Constant B	71.69	-

In order to validate the numerical rubber model with the experimental model, Mass of the tire debris model should weigh same as the experimental model to prove initial validation. Weight of the experimental tire debris model is 28 grams and the numerical model weighed 27.5 grams as shown in the figure 4.4.

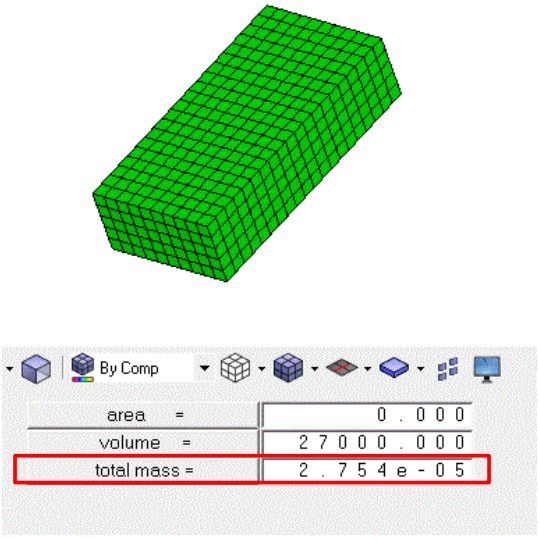

Figure 4.4 Weight of the numerical tire debris model displayed in tons.

4.2 Test Setup for Validation

Test setup configuration is shown in the figure 4.5. Tire debris model which is parallel to the horizontal plane is impacted on to the aluminum plate which is oriented at 30^0 from the horizontal plane. The tire debris model is impacted on aluminum plate with a velocity of 135 meters per seconds.

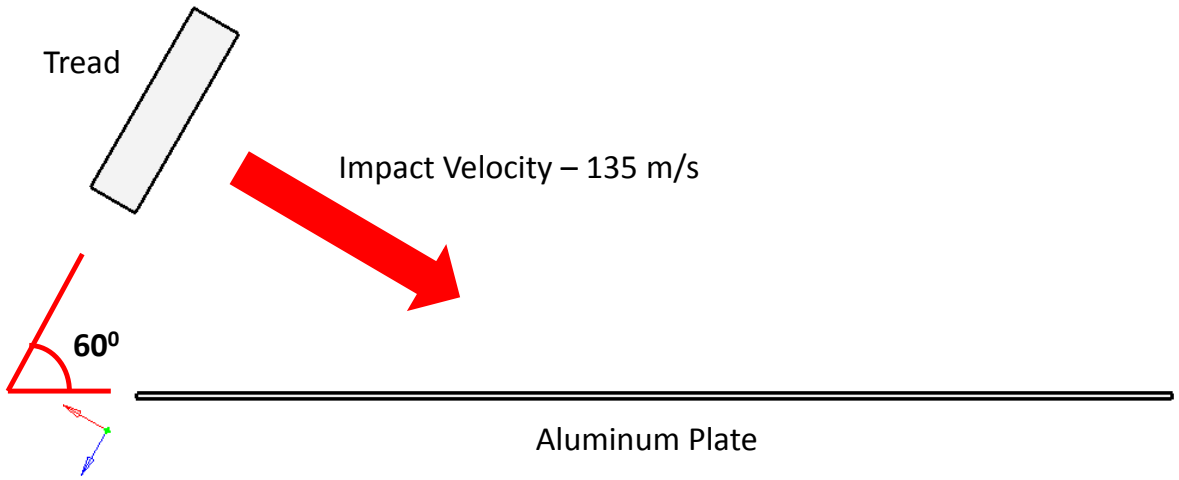

Figure 4.5 Test setup for validation test [23].

Strain gauges are located on the aluminum plate for calculating the strains in X and Y direction after the impact. Strain gauge 1 and 2 are located at the center of the plate which is 150 mm from the horizontal plane and 150 mm from the vertical plane. Strain gauge 3 is located at a distance of 250 mm from the horizontal plane and 150 mm from the vertical plane. Location of the strain gauges is shown in figure 4.6. Strain gauge 1 and 3 are used to calculate strains in vertical direction and strain gauge 2 calculates strain in horizontal direction.

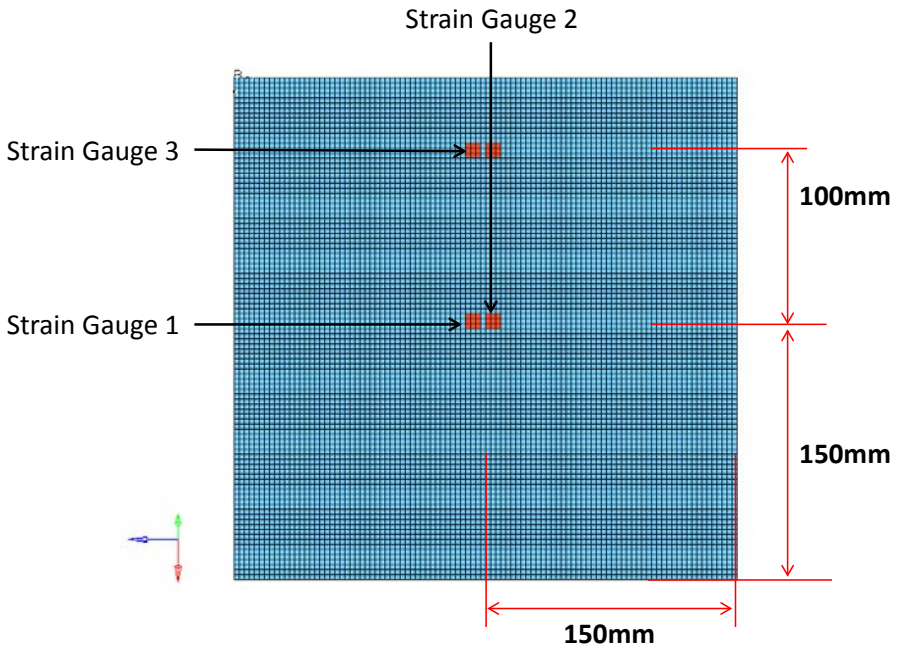

Figure 4.6 Location of strain gauges

4.3 Validation of the Tire Debris Model

Tire debris model is validated by impacting it on to the aluminum plate and comparing the numerical simulation results with the experimental results. Finite element mesh is checked for quality criteria in Hypermesh. LS Dyna contact definitions are assigned to the tire debris model and aluminum plate by assigning master and slave segments for the parts in the *CONTACT cards. Coefficient of friction values are assigned for the models from the reference [23]. Aluminum plate is constrained in X, Y and Z directions at the fastener locations. Impact velocity of 135 m/s is assigned to the tire debris model using *VELOCITY_GENERATION card in LS Dyna. After the simulation, results are post processed in Altair Hyperworks. Numerical simulation tends to follow the experimental test which is shown in figure 4.7.

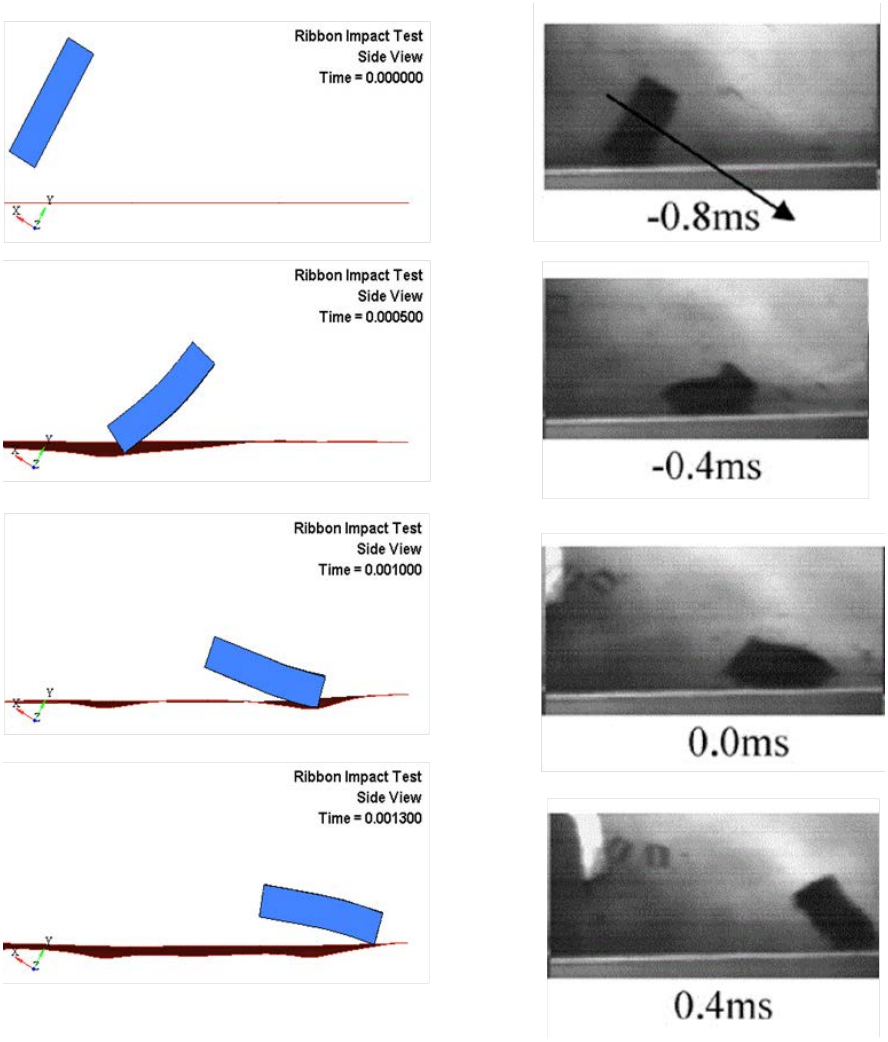

Figure 4.7 Comparison of numerical simulation with experimental test [23].

As the tire debris was impacted on to the aluminum plate which was angled 30^0 to the horizontal ground plane, rearward end of the tire debris model impacted exactly at the center of the aluminum plate at time 0.5 millisecond near strain gauge location 1 and 2. There was drop in kinetic energy for the tire debris model at this time. Tire debris model tend to follow the direction, slightly bends towards the front and the forward end of the tire debris model impacts aluminum plate at the strain gauge location 3.

4.3.1. Strain Results for Validation

Strains in X and Y directions are calculated from strain gauges located on the aluminum plate. Strains from numerical simulation and experimental test are overlaid on each other.

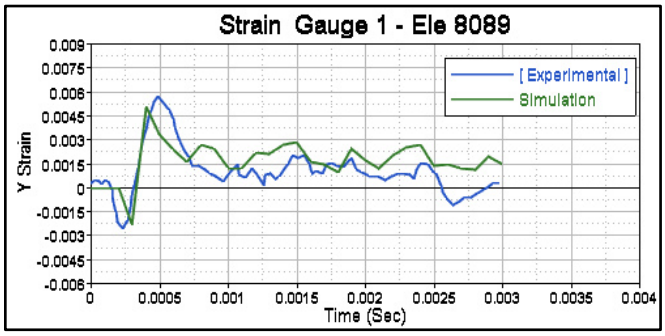

Figure 4.8 Strain in Y direction.

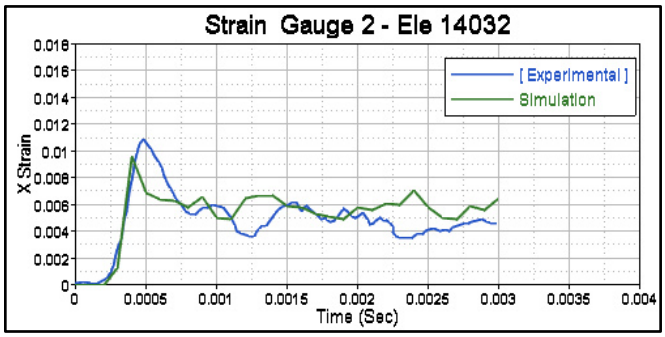

Figure 4.9 Strain in X direction.

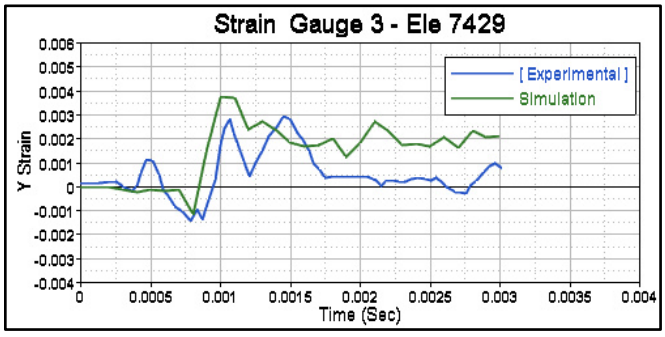

Figure 4.10 Strain in Y direction.

Strains are calculated in Y direction for the aluminum plate at strain gauge locations 1 and 3 from the experimental test [23]. Strains are calculated in Y direction for the elements 8089 and element 7429 from the numerical simulation which represents the strain gauge 1 and 3 as shown in the figures 4.8 and 4.10 respectively. Similarly strain in X direction is calculated for element 14032 from the numerical simulation which represents the strain gauge 2 as shown in the figure 4.9.

TABLE 4.2

VALUES OF STRAIN FROM STRAIN GAUGES [23]

Location	**Experiment**	**Simulation**
Strain Gauge 1	0.0053	0.0051
Strain Gauge 2	0.0098	0.0095
Strain Gauge 3	0.0028	0.0031

Values of the strains in Y and X directions for the strain gauges 1, 3 and 2 are calculated at the time when tire debris impacts at strain gauge locations. Experiment and simulation values are tabulated in table 4.1. A good correlation exits for experimental and numerical simulations with variation of 3%.

4.3.2. Energy Results for Validation

From the law of conservation of momentum, there will be a change in energy from one part to another after tire debris model impacts the aluminum plate. In order to validate the

process, the total system should have perfect energy balance i.e., energy ratio should be equal to 1. Energy ratio is defined as the ratio of total energy of the system to initial energy of the system [12]. Energy ratio of the analysis is shown in figure 4.11.

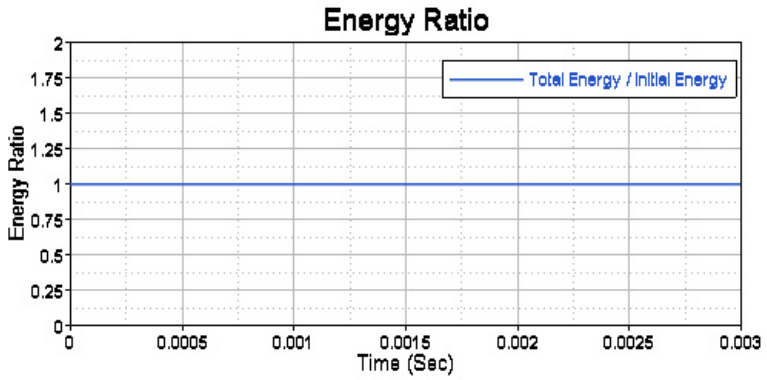

Figure 4.11 Energy ratio of the analysis.

After the tire debris model impacts aluminum plate, kinetic energy in the tire debris model is dropped from 251 N-m to 190 N-m. After the tire debris impacts the plate at second location, there is a gradual loss of kinetic energy from 182 N-m to 131 N-m. Overall loss of kinetic energy for the tire debris model is shown in the figure 4.12.

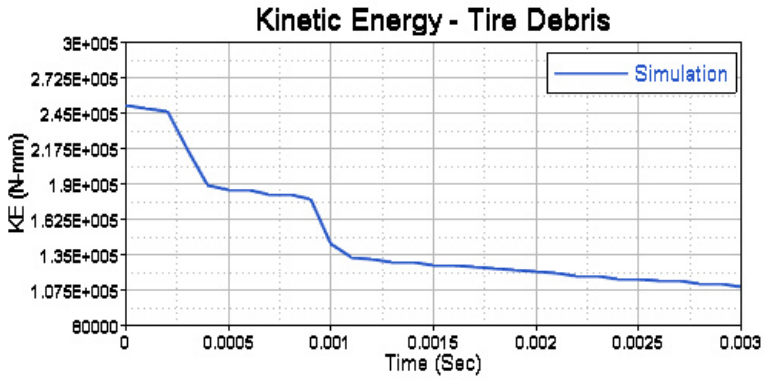

Figure 4.12 Kinetic Energy lost in the tire debris model.

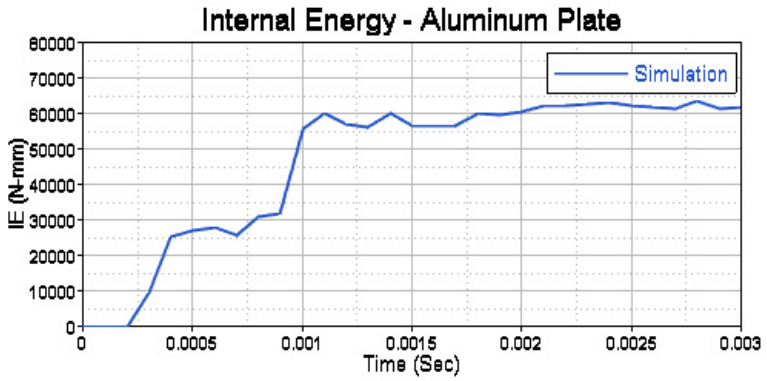

Figure 4.13 Internal Energy gained in the aluminum plate.

Similarly, internal energy in the tire debris model is increased from 0 N-m to 28 N-m when the tire debris impacts aluminum plate at first location. Gain in internal energy from 31 N-m to 60 N-m is observed as the tire debris impacts the plate at second location. Overall gain in internal energy for the tire debris model is shown in the figure 4.13.

CHAPTER 5

TIRE DEBRIS IMPACT ON INBOARD FLAP

5.1 Geometry of Inboard Flap

Geometry of inboard flap for a general aviation aircraft is designed using Catia V5 R21. All the dimensions and material properties for inboard flap assembly are taken from the references [4, 5 and 6]. Typical flap assembly for a general aviation aircraft consists of front spar, rear spar, ribs, stringers, tube structure, wing attachment structure and skin as shown in figure 5.1.

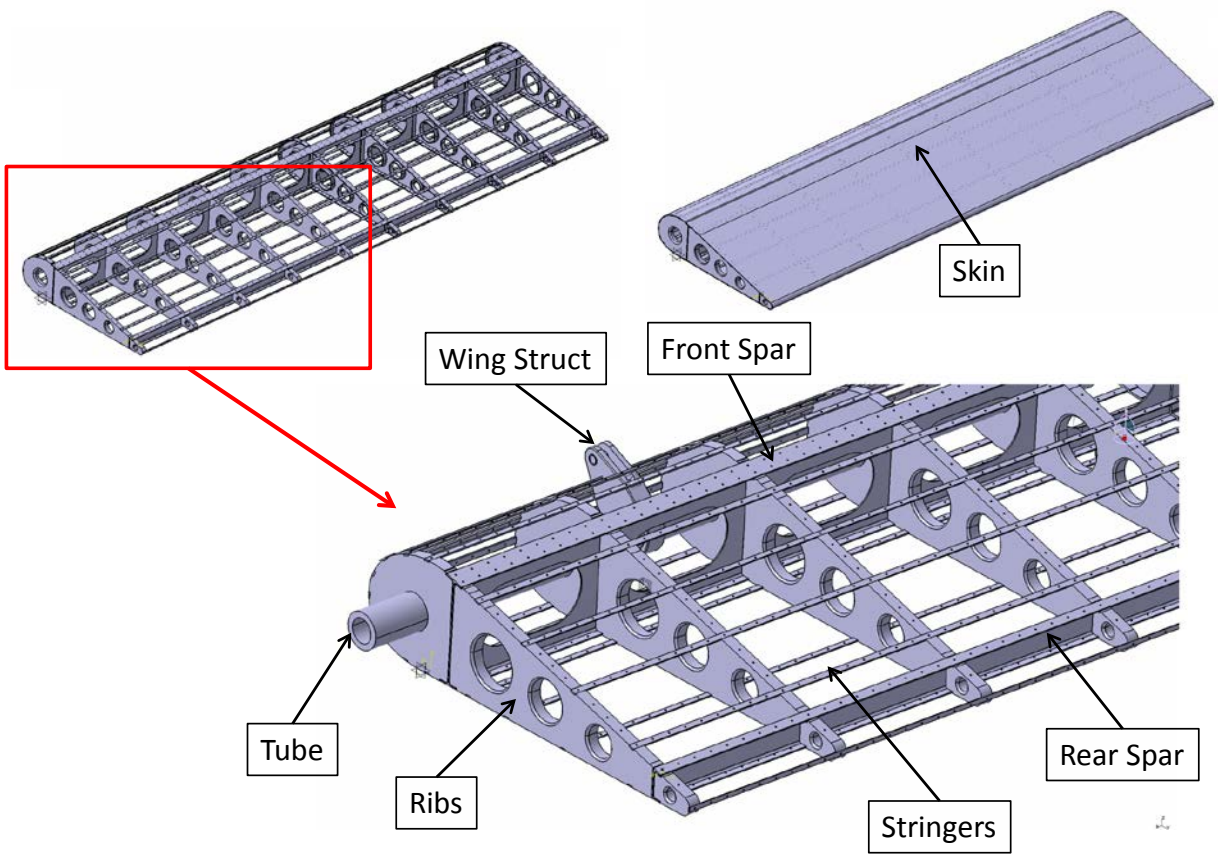

Figure 5.1 Geometry of inboard flap structure [4].

Michelin aircraft tire used for general aviation aircrafts is considered for this parametric study. The three part nomenclature of the tire is 17.5 X 5.75 -8. Where 17.5 is the nominal overall diameter for the tire in inches, 5.75 is the nominal section width of the tire in inches and 8 represents rim diameter in inches [26]. Complete tire has been designed and cross-section geometry is considered for parametric study as shown in figure 5.2. As per certification standards, small debris has to be used for validation of the structural parts. Small debris model should have mass equal to 1% mass of the whole aircraft tire. Michelin aircraft tire selected for the parametric study weighs 9.07 kg i.e. small debris should weigh 1% of the total mass, which would be 90.7 grams.

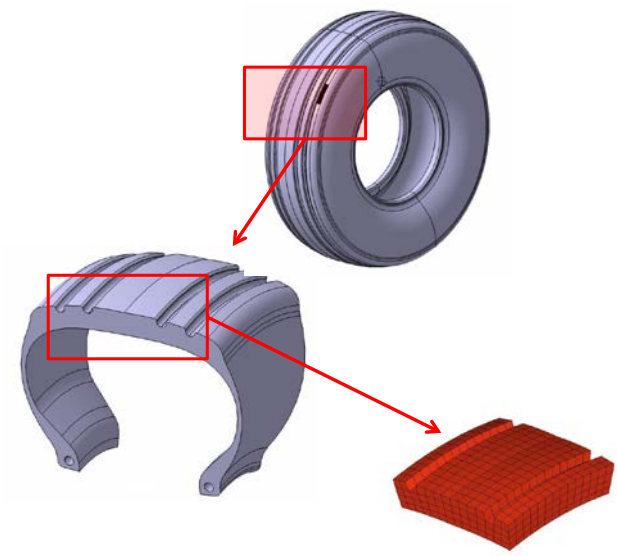

Figure 5.2 Cross-section geometry of the tire [26].

5.2 Finite Element Mesh of Inboard Flap

Before creating finite element mesh, geometry is cleaned up and mid surface planes are generated for the flap assembly components using Altair Hypermesh. Finite element mesh for

the structural parts consists of both shell mesh and solid mesh. Elements are checked for normal directions, element orientation and duplicates before the analysis. By maintaining good element quality criteria, more accurate results can be achieved by reducing errors for the analysis. A detailed mesh for the inboard flap assembly is shown in the figure 5.3.

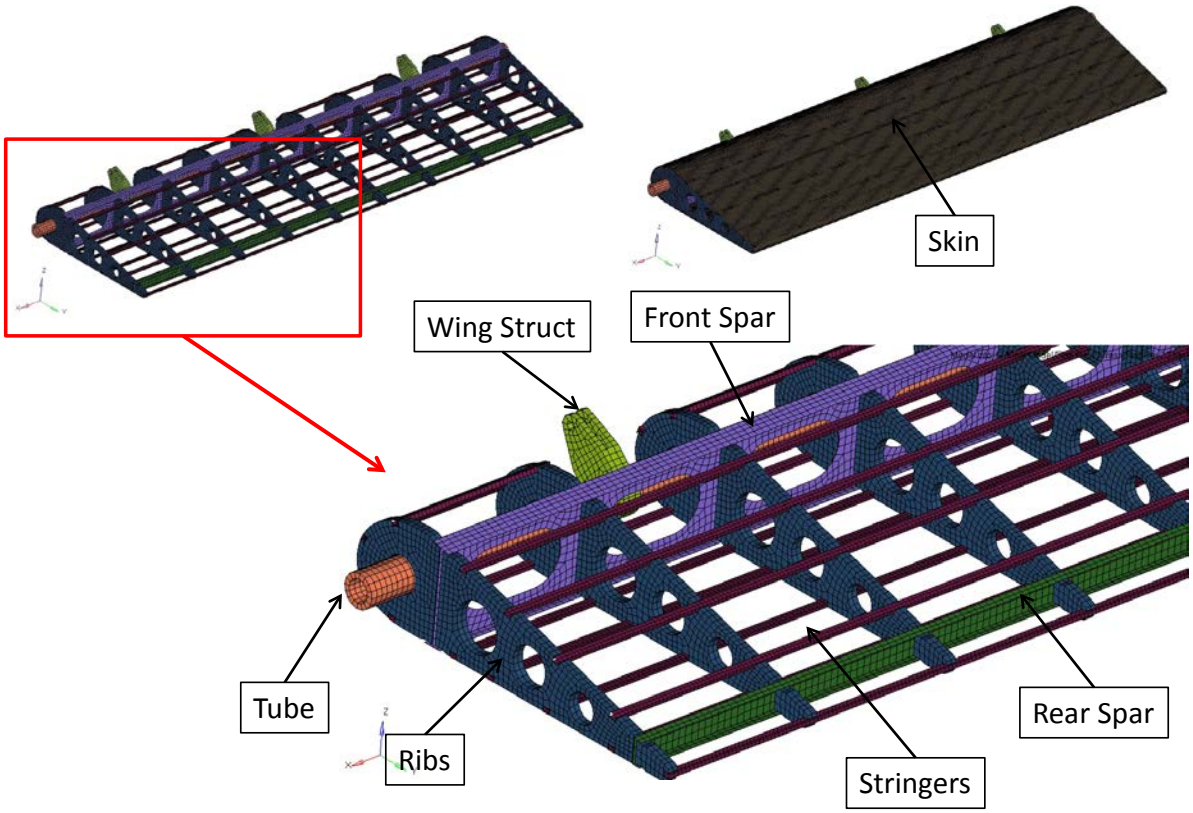

Figure 5.3 Finite element mesh of inboard flap assembly.

Fastener locations are shown in figure 5.4 which are modeled with beam elements. A total of 1858 beam elements, 121732 shell elements and 5572 solid elements are used in flap assembly model. Material properties are assigned to the parts using *MAT cards as shown in the table 5.1. Section properties are assigned to all the parts using *SECTION_SHELL and *SECTION_SOLID cards in LS Prepost. Automatic contact cards are assigned for all the parts

in flap assembly using *CONTACT_AUTOMATIC cards in LS Prepost. The flap assembly is constrained in X, Y, Z directions at the attachment points to the wing assembly using *BOUNDARY_SPC card. Velocity for the tire debris model is assigned using *INITIAL_VELOCITY card. *CONTROL cards are assigned for the model which includes the accuracy of the results, hourglass control and time step control. Output results are controlled by *ASCII and *D3PLOT from *DATABASE cards.

TABLE 5.1

MATERIAL DATA FOR INBOARD FLAP ASSEMBLY [4]

Part	**Material**	**Temper**	***MAT**	**Description**
Spar	AL 7075	T76	*MAT_81	Plasticity with damage
Ribs	AL 2024	T3	*MAT_81	Plasticity with damage
Stringers	AL 7075	T76	*MAT_81	Plasticity with damage
Tube	AL 2024	T3	*MAT_81	Plasticity with damage
Wing Struct	AL 2024	T351	*MAT_81	Plasticity with damage
Skin	AL 2024	T3	*MAT_81	Plasticity with damage
Tire Debris	Rubber 1450	-	*MAT_27	Mooney Rivlin Rubber
MS20470AD-2-6	AL 2117	T4	*MAT_100	Spotweld
MS20426DD-3-7	AL 2024	T42	*MAT_100	Spotweld
NAS1516-1522	AL 7075	T6	*MAT_100	Spotweld

5.3 Penetration Check for the Inboard Flap Assembly

All the parts in the flap assembly are connected at fastener locations using beam elements. A check must be done to find any unconstrained element in the model and also to find elements which are having part to part thickness penetrations and intersections. Flap assembly is dropped onto the rigid floor to at 5 meters per second to find any unconstrained beam elements and also for the part penetrations. Figure 5.4 shows the different time frames of the impact.

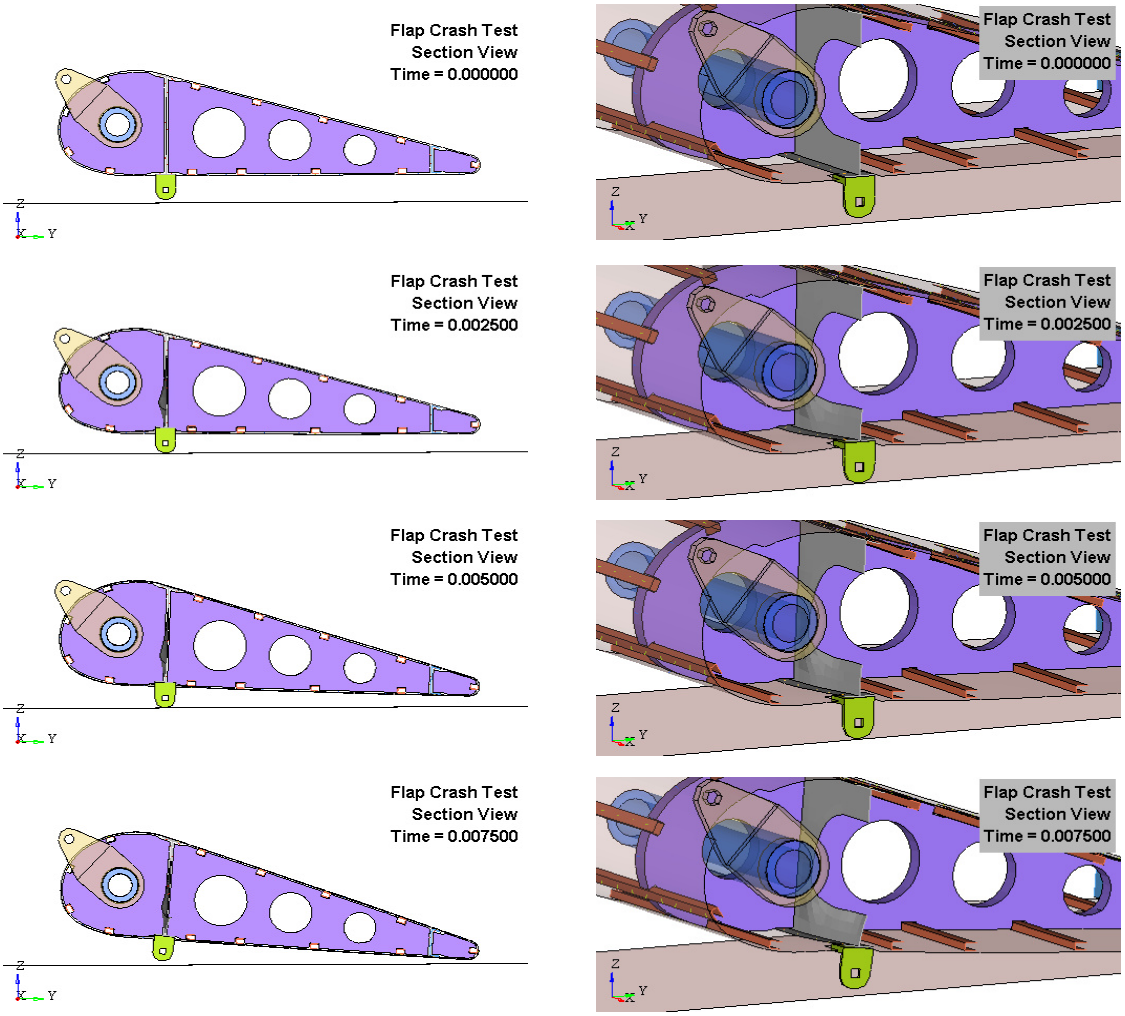

Figure 5.4 Penetration check for inboard flap.

5.4 Inboard Flap Impact Location 1

Impact location 1 is chosen to study deformations and energies in skin and stringer from flap assembly. After the tire burst, the probability of the tire debris impacting the flap at location 1 is high. Tire debris model impacting inboard flap at location 1 is shown in the figure 5.5. Parametric study is carried out by impacting tire debris model weighing 90.5 grams onto the inboard flap at location 1 with a velocity of 94 m/s and 135 m/s. 94 m/s is the manufacturer's recommended maximum speed of the tire on ground, 135 m/s is used to observe the behavior of structural components during the impact. Axial and shear forces are measured for the fasteners in this location to study the behavior of fastener failure. Kinetic energy and internal energy for the major structural parts being impacted are plotted. Deformations on the skin for location 1 after the impact are calculated and compared with different cases.

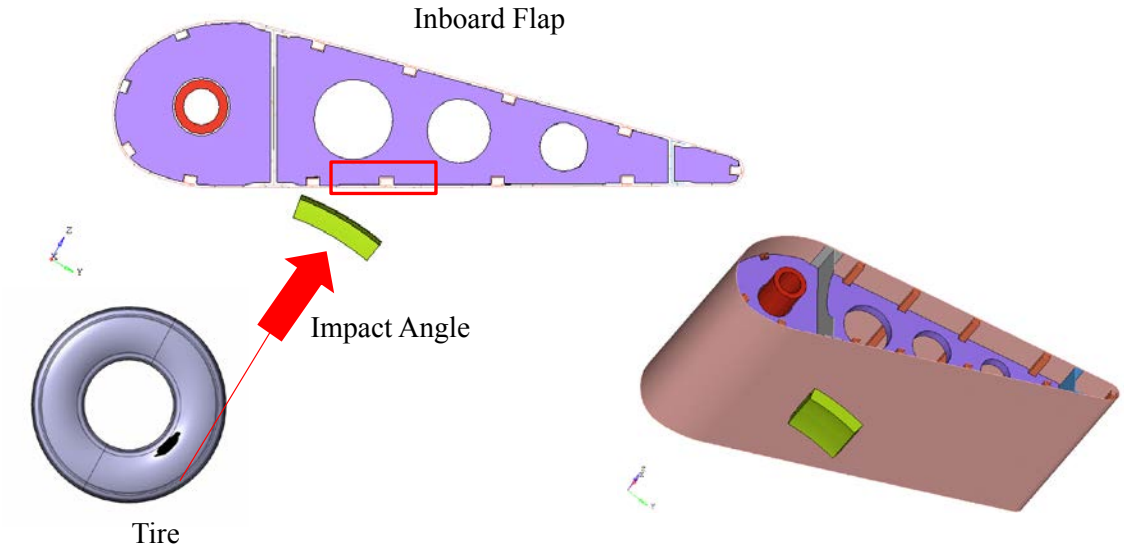

Figure 5.5 Location 1 for flap impact model.

5.4.1. Inboard Flap at 0^0 Angle of Attack

In this case, validated tire debris model is impacted onto the inboard flap which is oriented at 0^0 to the ground plane with velocities of 94 m/s and 135 m/s.

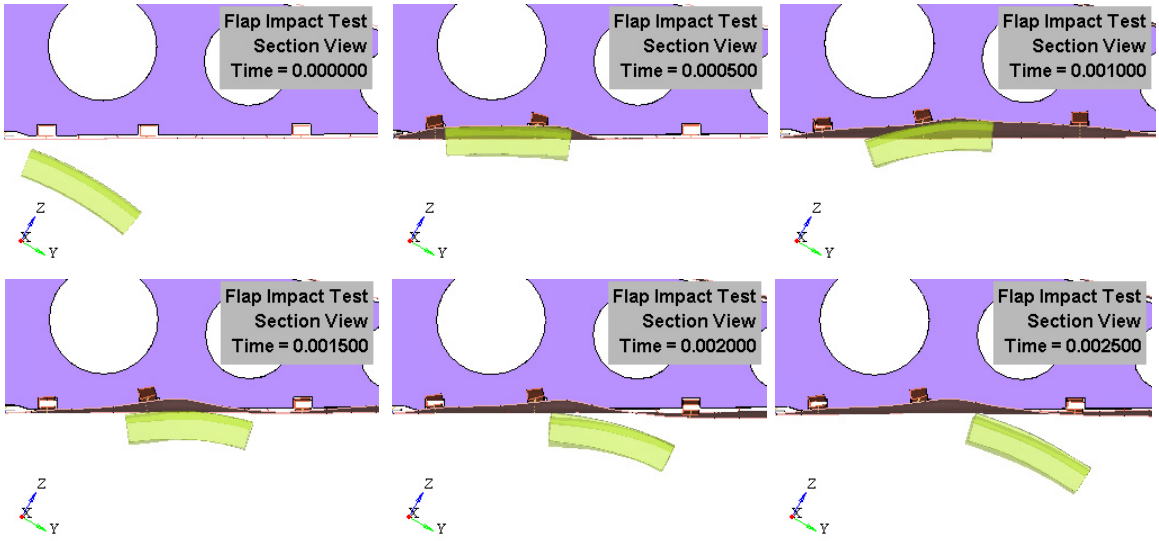

Figure 5.6 Time frames of the impact with a velocity of 94 m/s.

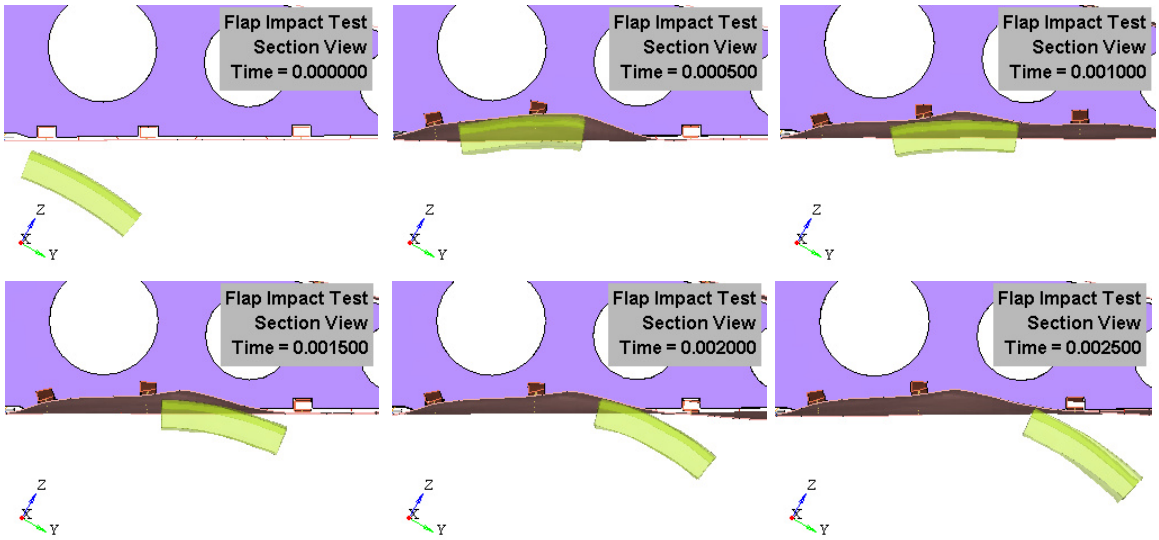

Figure 5.7 Time frames of the impact with a velocity of 135 m/s.

Time frames for the impact of tire debris onto the flap with velocity of 94 m/s are shown in the figure 5.6 and time frames for the impact of tire debris onto the flap with velocity of 135 m/s are shown in the figure 5.7. More deformation can be observed in the stringer located in the impact zone when impacted by tire debris at 135 m/s.

Effective plastic strain for the skin is calculated after the impact with tire debris for the two velocity cases as shown in the figure 5.8. Higher plastic strain of 0.1307 is observed in the skin impacted by tire debris with a velocity of 135 m/s. More percentage of plastic strain is observed in the skin impacted with high velocity.

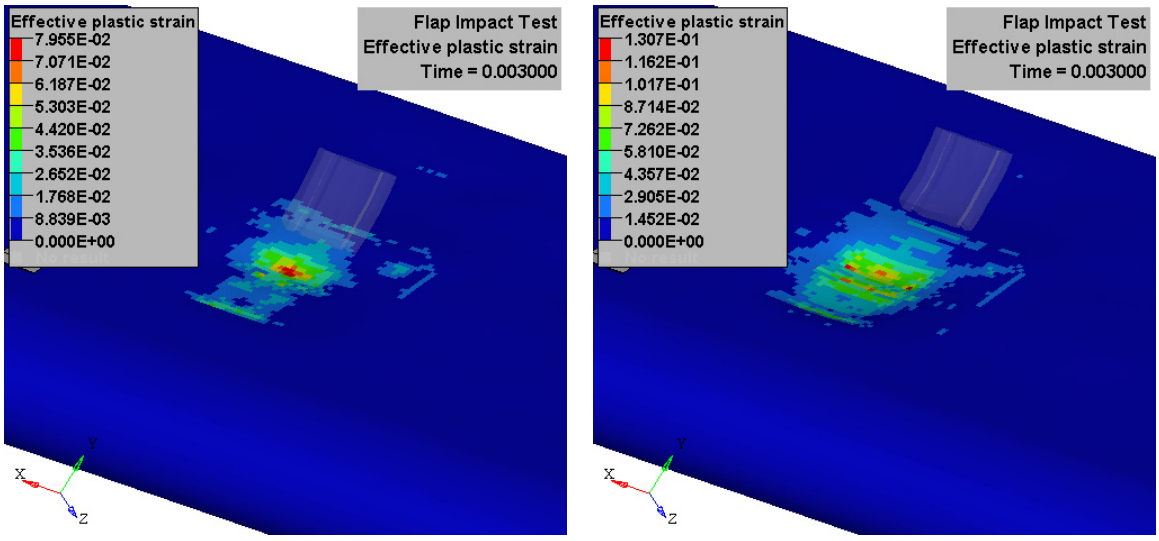

Figure 5.8 Effective plastic strains in the skin impacted by tire debris with 94 m/s and 135 m/s.

Stress distributions on the skin impacted by tire debris with 94 m/s and 135 m/s are shown in the figure 5.9 and 5.10 respectively. High regime of stress distribution is observed on the skin during impact time of 0.6 milliseconds. In the case of tire debris impacting with 94 m/s, stress of 435 MPa is calculated on the skin. But in the case of tire debris impacting with 135 m/s, stress of 494 MPa is calculated on the skin.

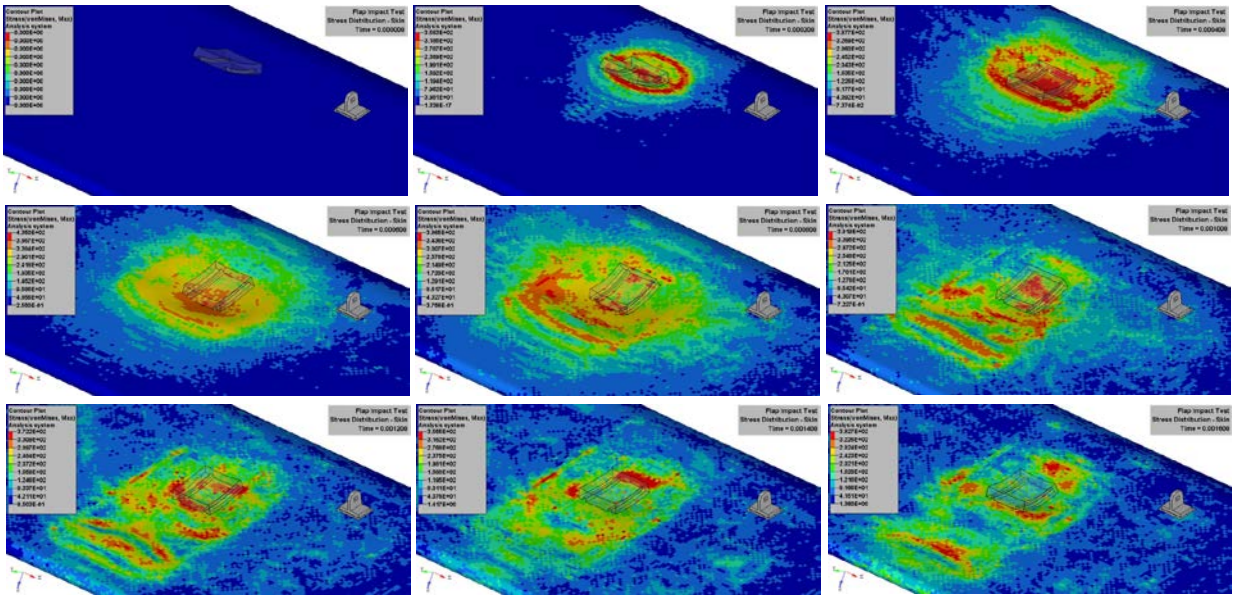

Figure 5.9 Stress distributions on the skin impacted by tire debris with 94 m/s.

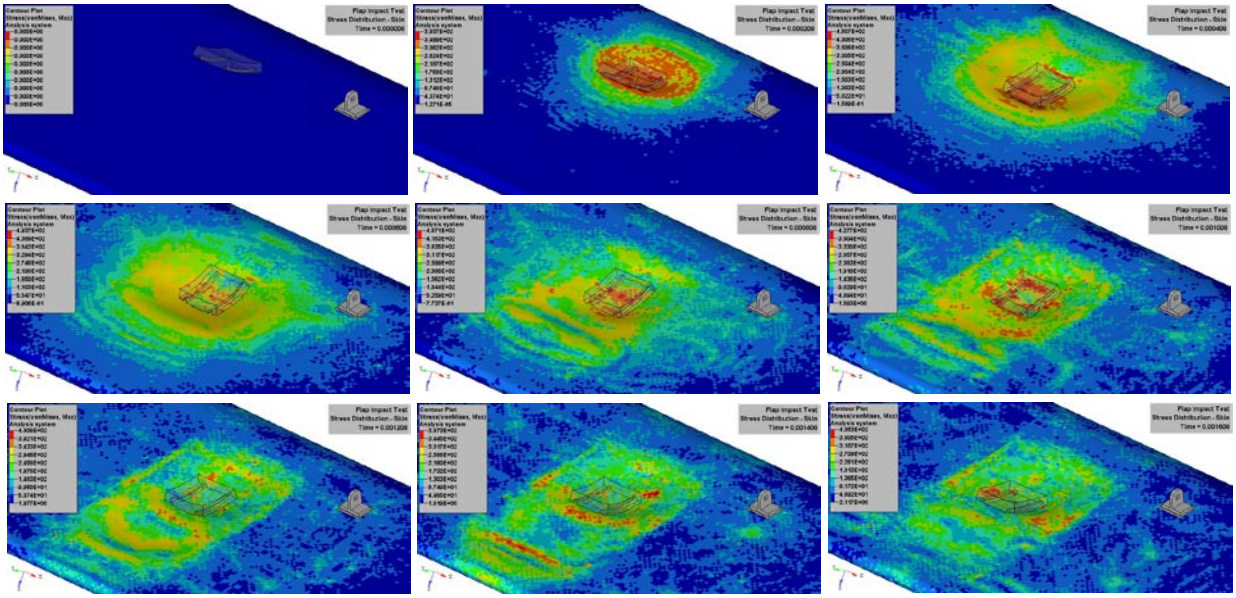

Figure 5.10 Stress distributions on the skin impacted by the tire debris with 135 m/s.

5.4.2. Inboard Flap at 10^0 Angle of Attack

In this case, validated tire debris model is impacted onto the inboard flap which is oriented at 10^0 to the ground plane with velocities of 94 m/s and 135 m/s.

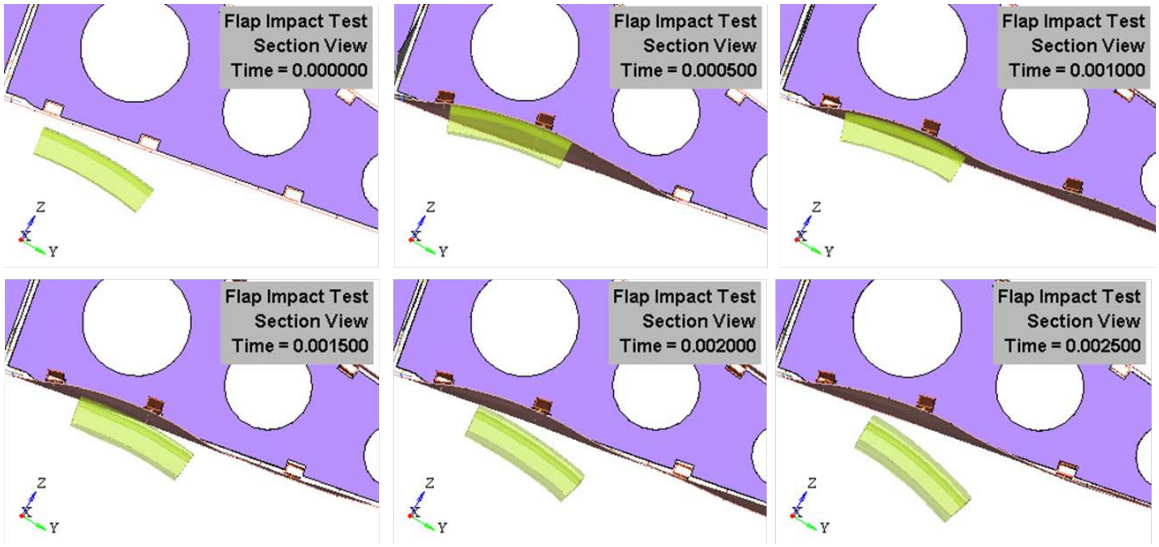

Figure 5.11 Time frames of the impact with a velocity of 94 m/s.

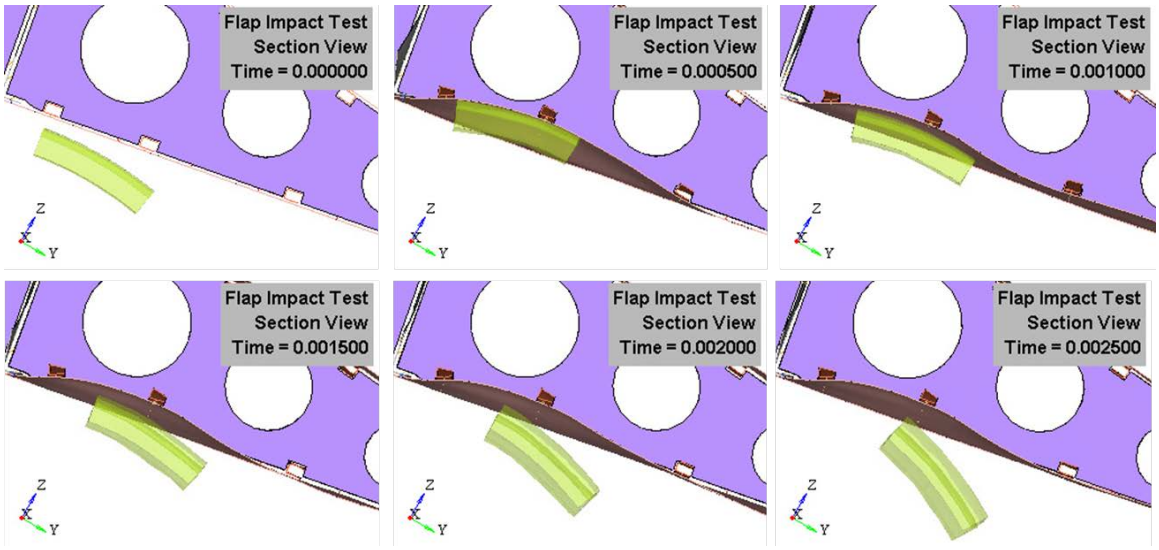

Figure 5.12 Time frames of the impact with a velocity of 135 m/s.

Time frames for the impact of tire debris on to the flap with velocity of 94 m/s are shown in the figure 5.11 and time frames for the impact of tire debris on to the flap with velocity of 135 m/s are shown in the figure 5.12. More deformation can be observed in the stringer located in the impact zone when impacted by tire debris at 135 m/s.

Effective plastic strain for the skin is calculated after the impact with tire debris for the two velocity cases as shown in the figure 5.13. Higher plastic strain of 0.0967 is observed in the skin impacted by tire debris with a velocity of 135 m/s. Percentage of plastic strain observed in the skin impacted with high velocity and low velocity remains same when flap is oriented at 10^0 to the ground horizontal.

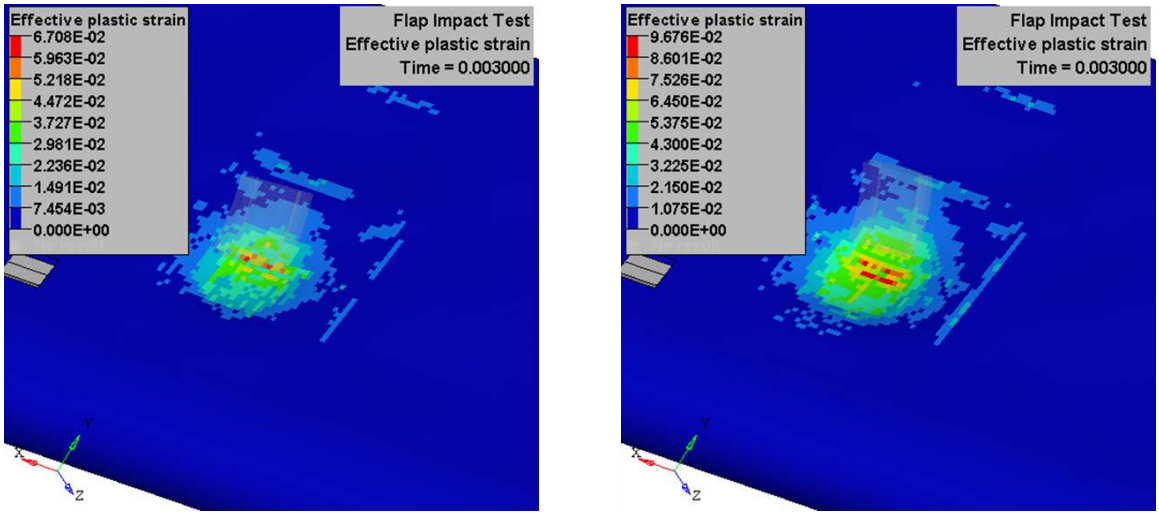

Figure 5.13 Effective plastic strains in the skin impacted by tire debris with 94 m/s & 135 m/s.

Stress distributions on the skin impacted by tire debris with 94 m/s and 135 m/s are shown in the figure 5.14 and 5.15 respectively. High regime of stress distribution is observed on the skin during impact time of 0.4milliseconds. In the case of tire debris impacting with 94 m/s, stress of 400 MPa is calculated on the skin. But in the case of tire debris impacting with

135 m/s, stress of 460 MPa is calculated on the skin.

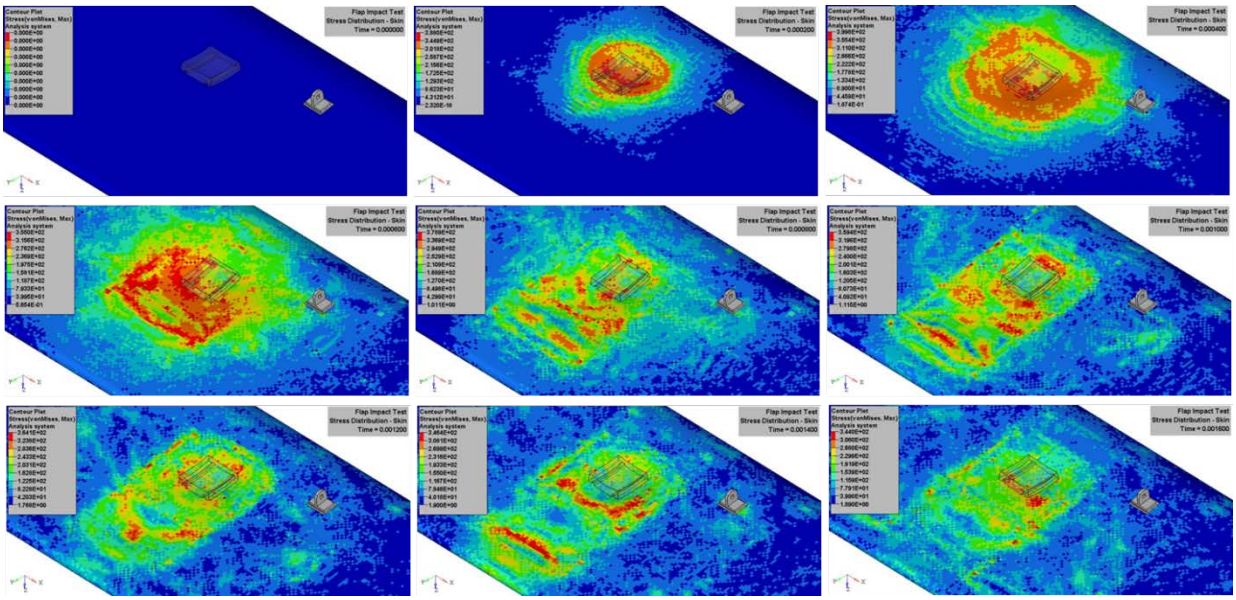

Figure 5.14 Stress distributions on the skin impacted by tire debris with 94 m/s.

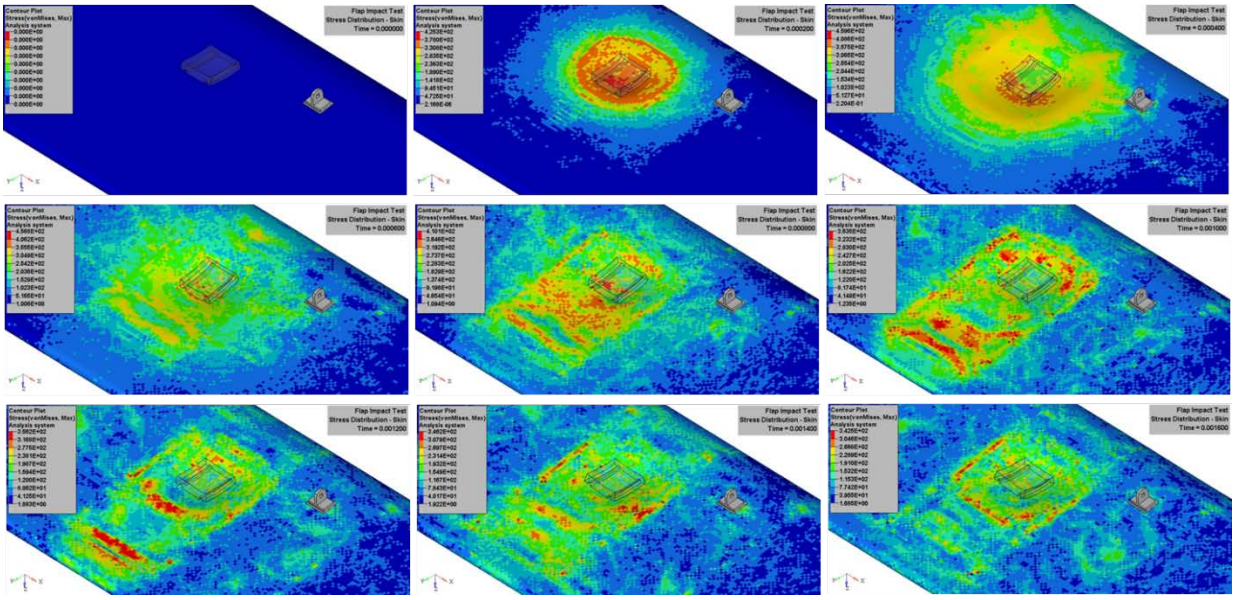

Figure 5.15 Stress distributions on the skin impacted by the tire debris with 135 m/s.

5.4.3. Inboard Flap at 37^0 Angle of Attack

In this case, validated tire debris model is impacted onto the inboard flap which is oriented at 37^0 to the ground plane with velocities of 94 m/s and 135 m/s.

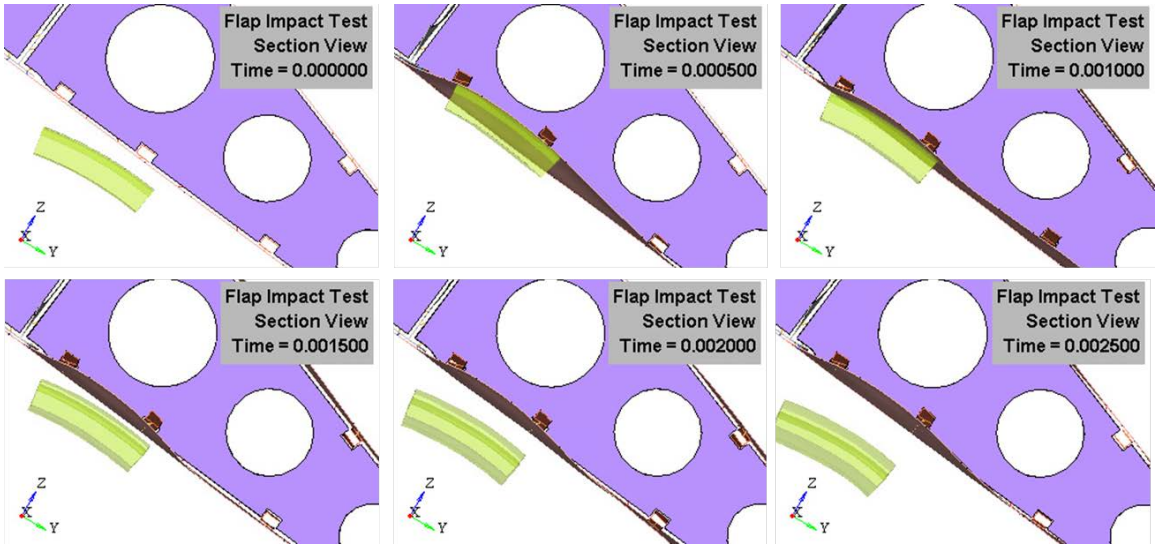

Figure 5.16 Time frames of the impact with a velocity of 94 m/s.

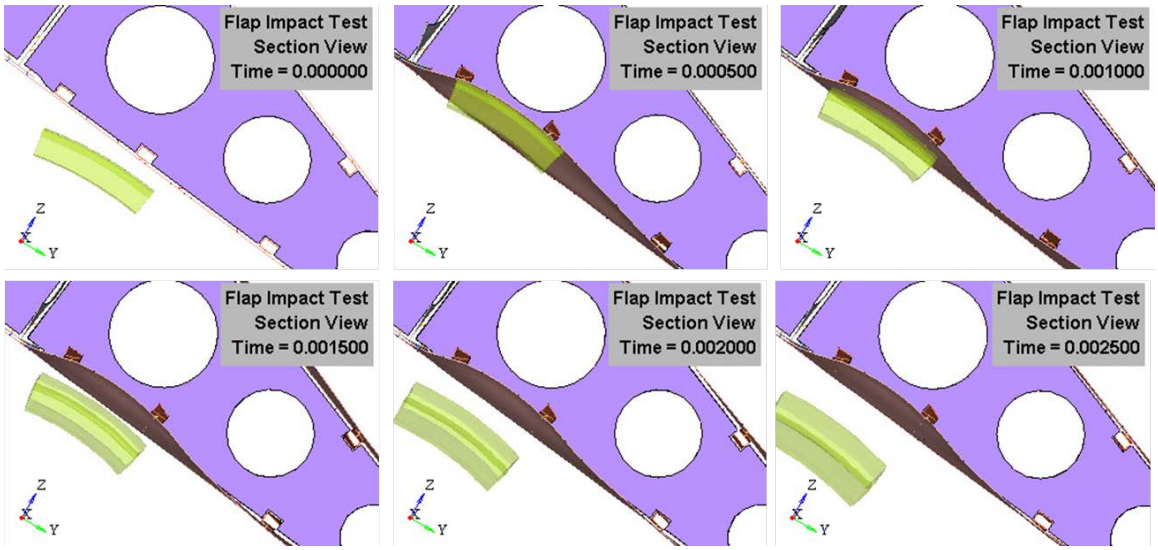

Figure 5.17 Time frames of the impact with a velocity of 135 m/s.

Time frames for the impact of tire debris on to the flap with velocity of 94 m/s are shown in the figure 5.16 and time frames for the impact of tire debris on to the flap with velocity of 135 m/s are shown in the figure 5.17. More deformation can be observed in the stringer located in the impact zone when impacted by tire debris at 135 m/s.

Effective plastic strain for the skin is calculated after the impact with tire debris for the two velocity cases as shown in the figure 5.18. Higher plastic strain of 0.0907 is observed in the skin impacted by tire debris with a velocity of 135 m/s. Percentage of plastic strain observed in the skin impacted with high velocity and low velocity remains same when flap is oriented at 37^0 to the ground horizontal.

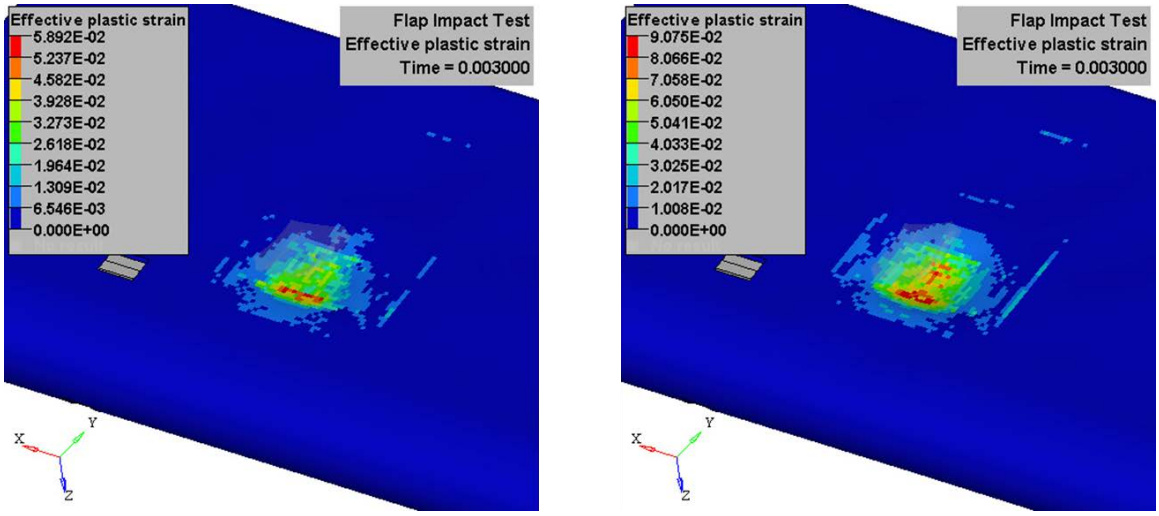

Figure 5.18 Effective plastic strains in the skin impacted by tire debris with 94 m/s & 135 m/s.

Stress distributions on the skin impacted by tire debris with 94 m/s and 135 m/s are shown in the figure 5.19 and 5.20 respectively. High regime of stress distribution is observed on the skin during impact time of 0.4 milliseconds. In the case of tire debris impacting with 94 m/s, stress of 400 MPa is calculated on the skin. But in the case of tire debris impacting with

135 m/s, stress of 436 MPa is calculated on the skin.

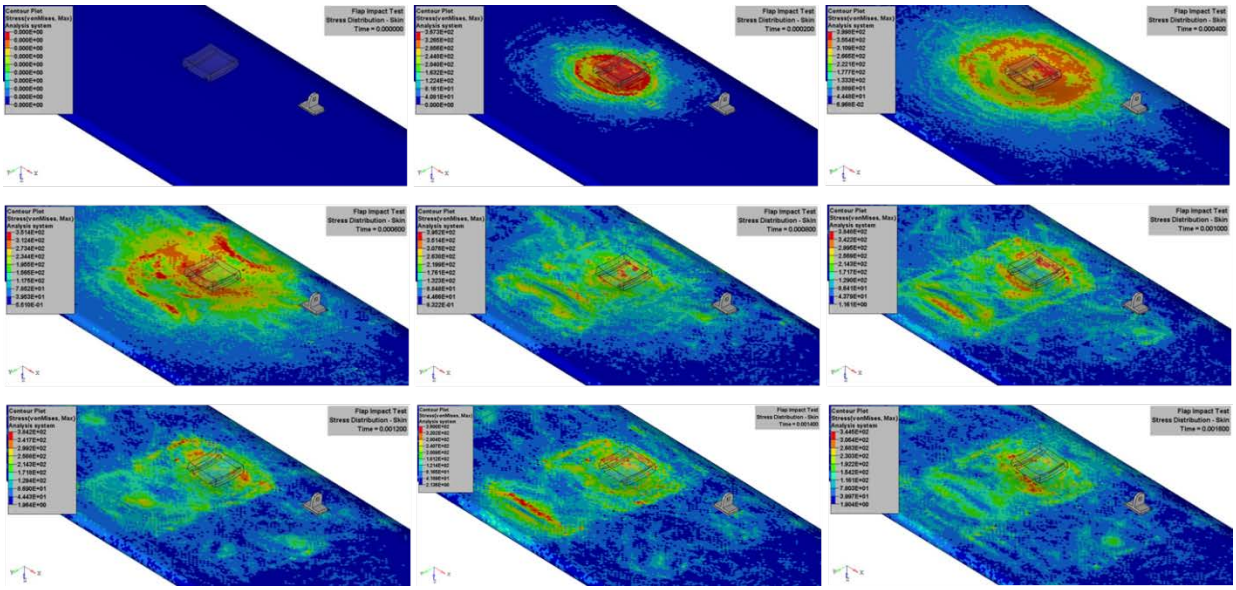

Figure 5.19 Stress distributions on the skin impacted by tire debris with 94 m/s.

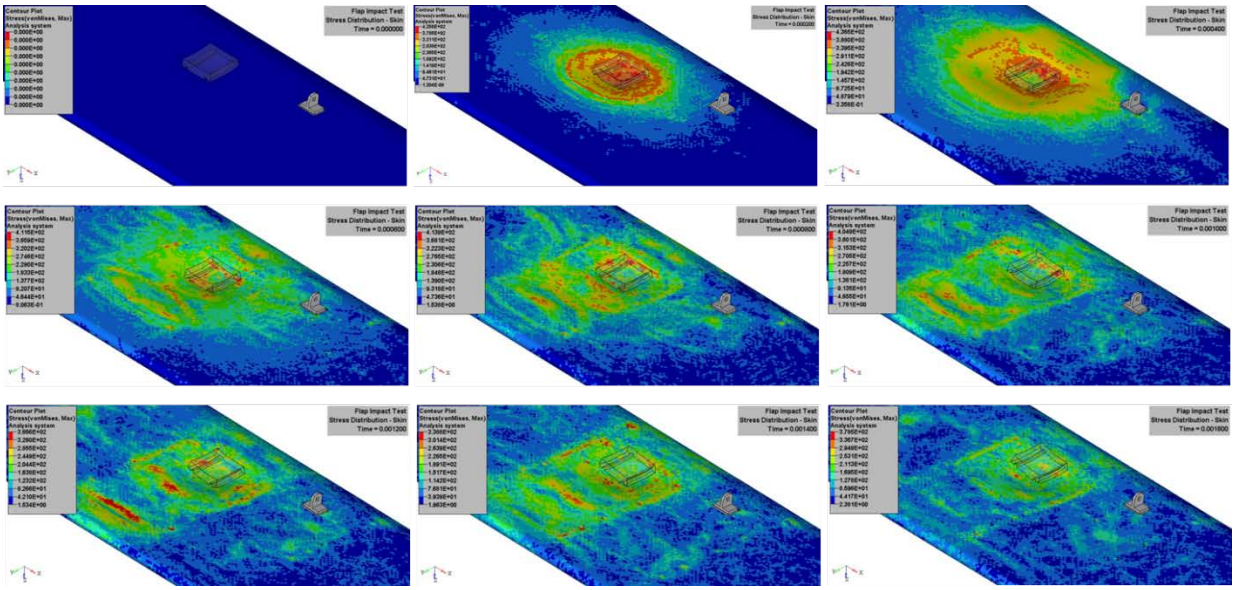

Figure 5.20 Stress distributions on the skin impacted by the tire debris with 135 m/s.

5.4.4. Energy Results for Flap Impact Analysis

Kinetic energies and internal energies are calculated for all the cases of flap impact analysis at location 1. Ratio of total energy of the system to initial energy of the system is equal to 1 as shown in the figure 5.21.

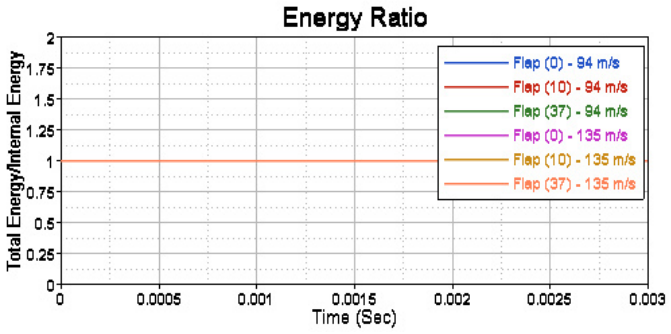

Figure 5.21 Energy Ratio of the system.

After the tire debris is impacted at location 1, its kinetic energy is transferred onto the skin and stringers located at impact location. Kinetic energy is lost in the tire debris model after it impacts the inboard flap assembly. Kinetic energy in the tire debris for all the six impact cases can be seen in figure 5.22. It can be noted that when tire debris impacts flap oriented at 10^0 and 37^0, they have the same amount of kinetic energy loss.

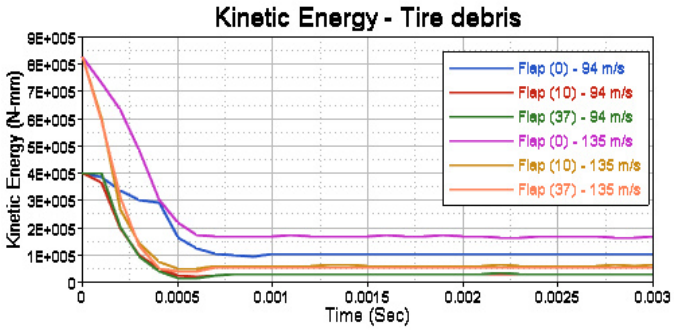

Figure 5.22 Kinetic Energy in tire debris model.

Internal energy gained in structural parts of stringers and skin is show in figure 5.23 and figure 5.24 respectively. After tire debris impacts stringer, internal energy is increased gradually for flap oriented at 0^0. More internal energy can be observed in the stringer when tire debris impacts the flap oriented at 37^0.

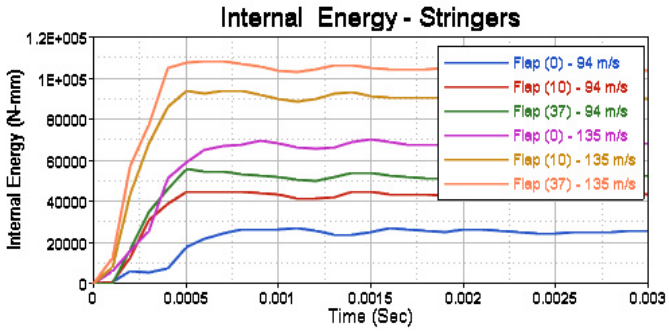

Figure 5.23 Internal Energy in the stringers.

Internal energy in the skin increases gradually for the flap at 0^0, but for the flap at 37^0 there is sudden increase in energy as the tire debris impacts almost perpendicular to the skin. A huge difference in internal energies for the skin can be observed when the tire debris impacts at 94 m/s and 135 m/s.

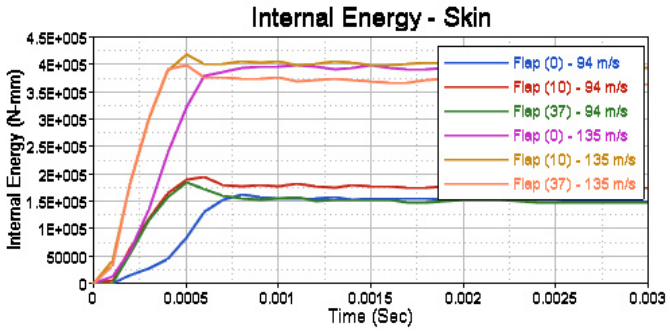

Figure 5.24 Internal Energy in the skin.

5.5 Inboard Flap Impact Location 2

Impact location 2 is chosen to study deformations and energies in skin, rear spar and stringer. After the tire burst, there is the probability of the tire debris impacting the flap at location 2. Tire debris model impacting inboard flap at location 2 is shown in the figure 5.25. Parametric study is done by impacting tire debris model weighing 90.5 grams on to the inboard flap at location 2 with a velocity of 94 m/s and 135 m/s. 94 m/s is the manufacturer's recommended maximum speed of the tire on ground, 135 m/s is used to observe the behavior of structural components during the impact. Axial and shear forces are measured for the fasteners in this location to study the behavior of fastener failure. Kinetic energy and internal energy for the major structural parts being impacted are plotted. Deformations on the skin for location 2 after the impact is calculated and compared with different cases.

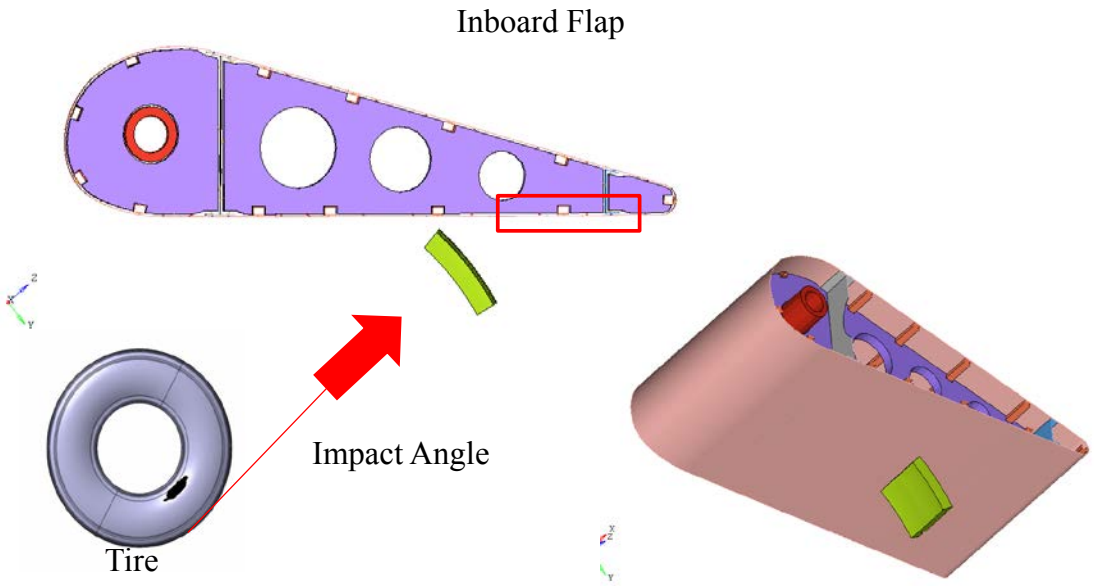

Figure 5.25 Location 2 for flap impact model.

5.5.1. Inboard Flap at 0^0 Angle of Attack

In this case, validated tire debris model is impacted onto the inboard flap which is oriented at 0^0 to the ground plane with velocities of 94 m/s and 135 m/s.

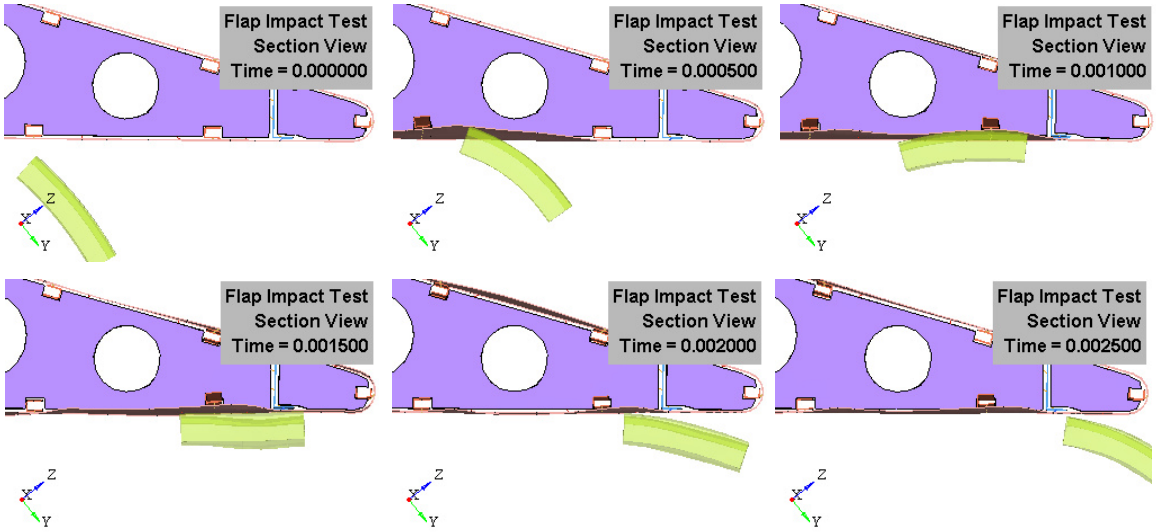

Figure 5.26 Time frames of the impact with a velocity of 94 m/s.

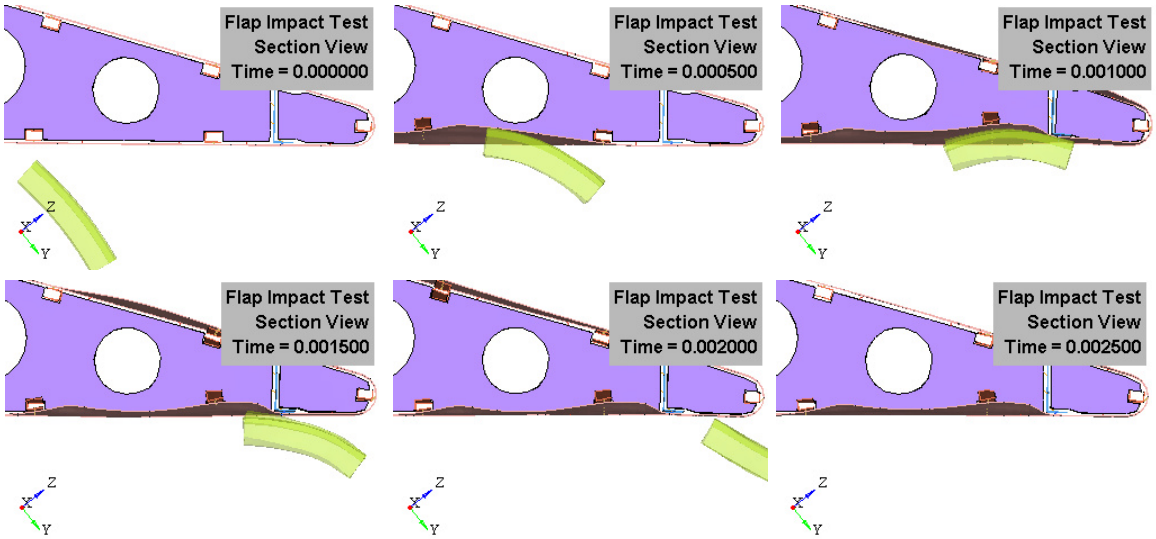

Figure 5.27 Time frames of the impact with a velocity of 135 m/s.

Time frames for the impact of tire debris on to the flap with velocity of 94 m/s are shown in the figure 5.26 and time frames for the impact of tire debris on to the flap with velocity of 135 m/s are shown in the figure 5.27. More deformation can be observed in the skin and stringer located in the impact zone when impacted by tire debris at 135 m/s.

Effective plastic strain for the skin is calculated after the impact with tire debris for the two velocity cases as shown in the figure 5.28. Higher plastic strain of 0.1432 is observed in the skin impacted by tire debris with a velocity of 135 m/s. More percentage of plastic strain is observed in the skin impacted with low velocity.

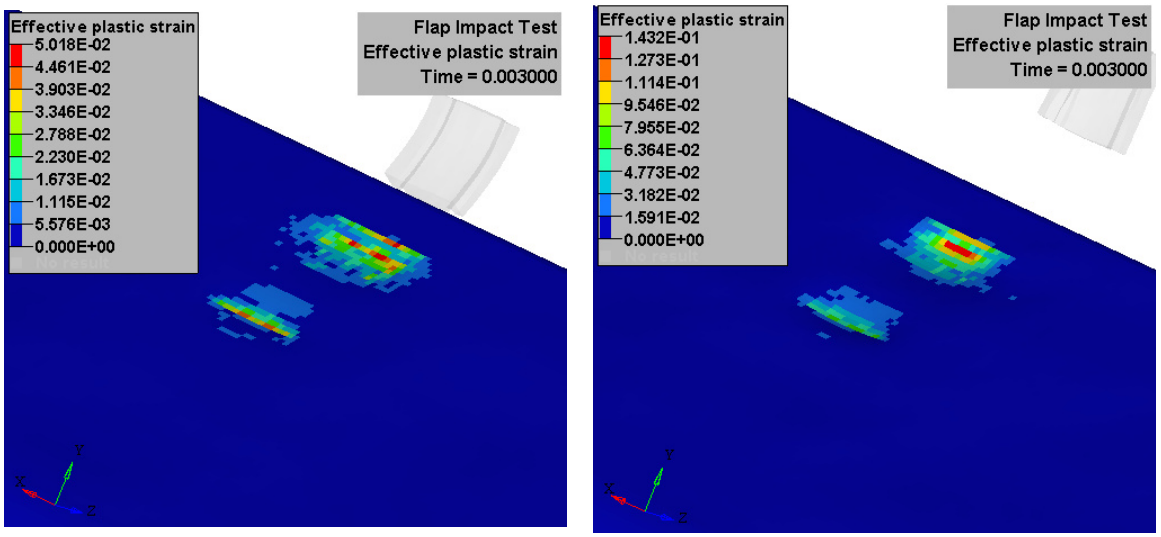

Figure 5.28 Effective plastic strains in the skin impacted by tire debris with 94 m/s and 135 m/s.

Stress distributions on the skin impacted by tire debris with 94 m/s and 135 m/s are shown in the figure 5.29 and 5.30 respectively. High regime of stress distribution is observed on the skin during impact time of 1.2 milliseconds. In the case of tire debris impacting with 94 m/s, stress of 388 MPa is calculated on the skin. But in the case of tire debris impacting with 135 m/s, high stress of 375 MPa is observed on the skin.

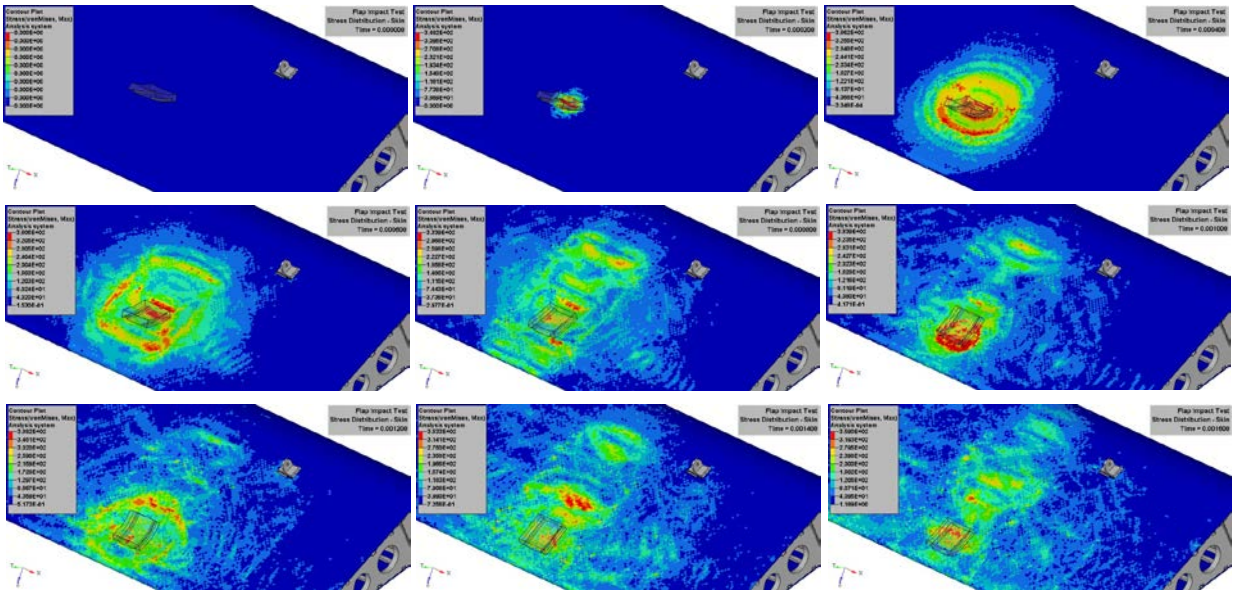

Figure 5.29 Stress distributions on the skin impacted by tire debris with 94 m/s.

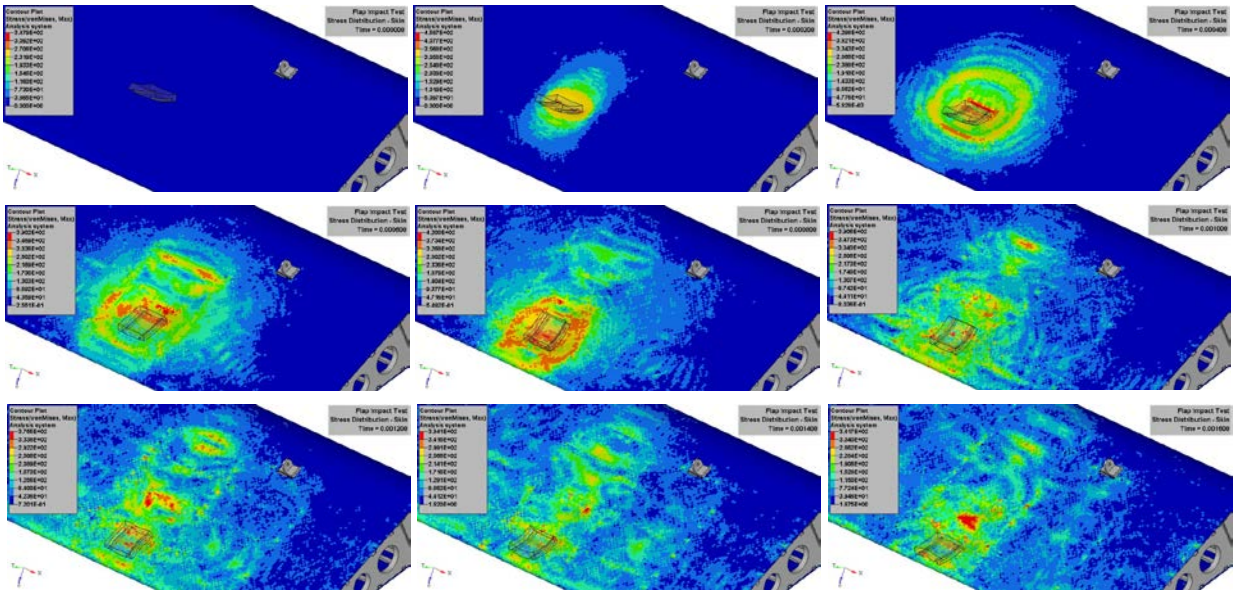

Figure 5.30 Stress distributions on the skin impacted by the tire debris with 135 m/s.

5.5.2. Inboard Flap at 10^0 Angle of Attack

In this case, validated tire debris model is impacted onto the inboard flap which is oriented at 10^0 to the ground plane with velocities of 94 m/s and 135 m/s.

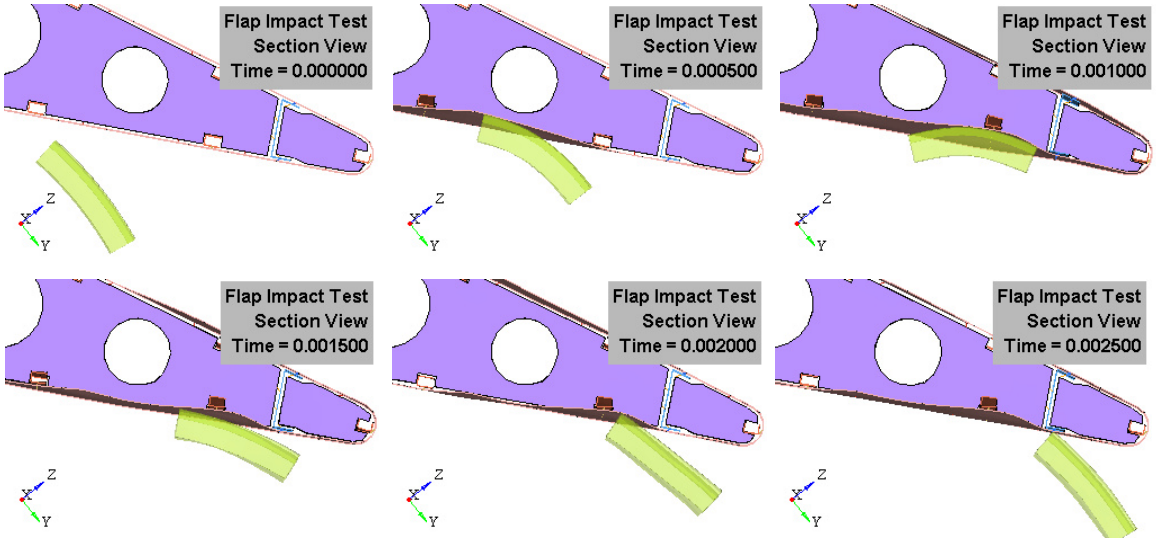

Figure 5.31 Time frames of the impact with a velocity of 94 m/s.

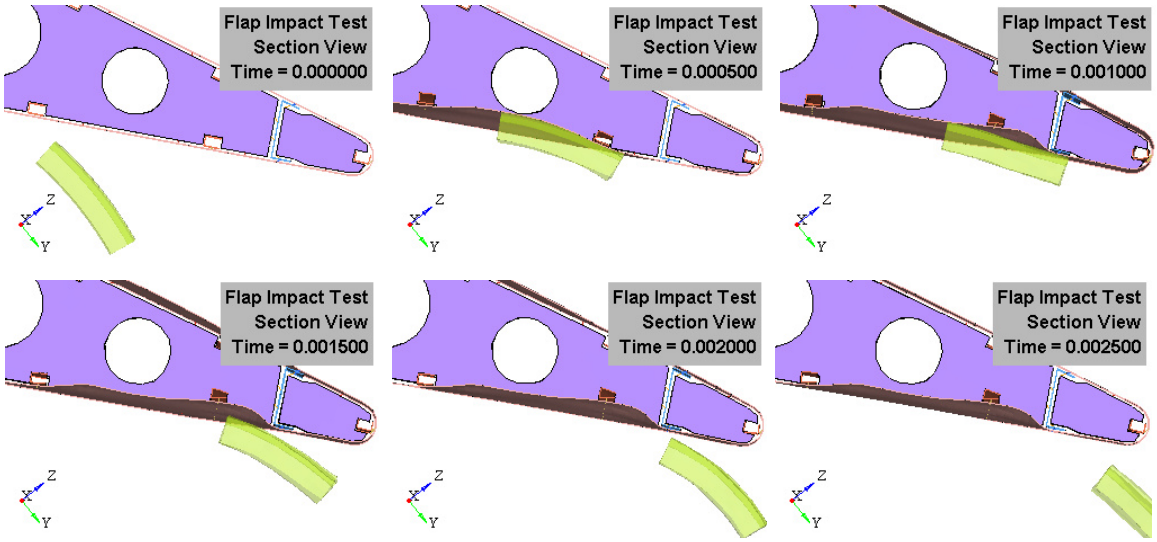

Figure 5.32 Time frames of the impact with a velocity of 135 m/s.

Time frames for the impact of tire debris on to the flap with velocity of 94 m/s are shown in the figure 5.31 and time frames for the impact of tire debris on to the flap with velocity of 135 m/s are shown in the figure 5.32. More deformation can be observed in the stringer and skin located in the impact zone when impacted by tire debris at 135 m/s.

Effective plastic strain for the skin is calculated after the impact with tire debris for the two velocity cases as shown in the figure 5.33. Higher plastic strain of 0.1465 is observed in the skin impacted by tire debris with a velocity of 135 m/s. Percentage of plastic strain observed in the skin impacted with high velocity and low velocity remains almost the same when flap is oriented at 10^0 to the ground horizontal.

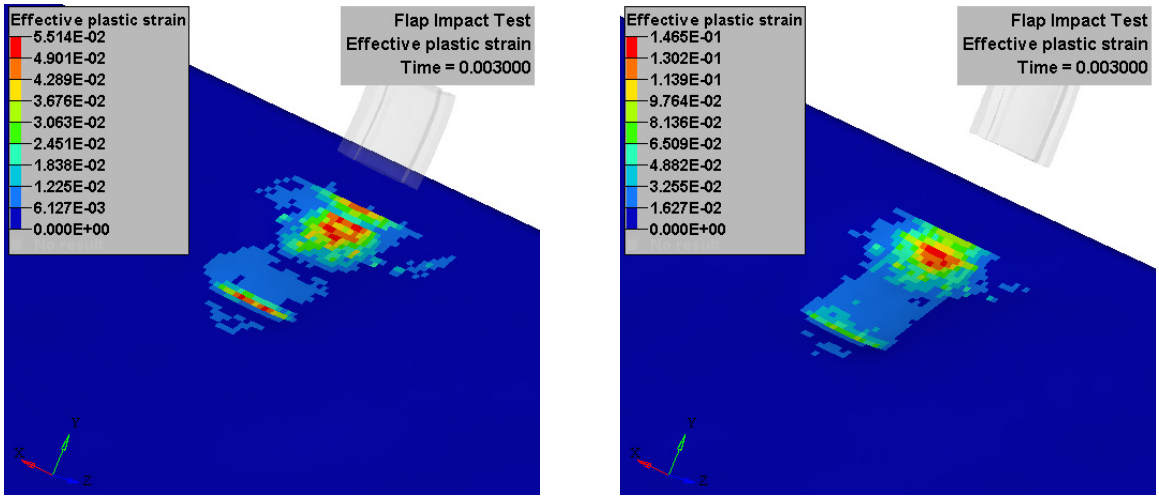

Figure 5.33 Effective plastic strains in the skin impacted by tire debris with 94 m/s & 135 m/s.

Stress distributions on the skin impacted by tire debris with 94 m/s and 135 m/s are shown in the figure 5.34 and 5.35 respectively. High regime of stress distribution is observed on the skin during impact time of 0.8milliseconds. In the case of tire debris impacting with 94 m/s, stress of 398 MPa is calculated on the skin. But in the case of tire debris impacting with 135 m/s, stress of 497 MPa is calculated on the skin.

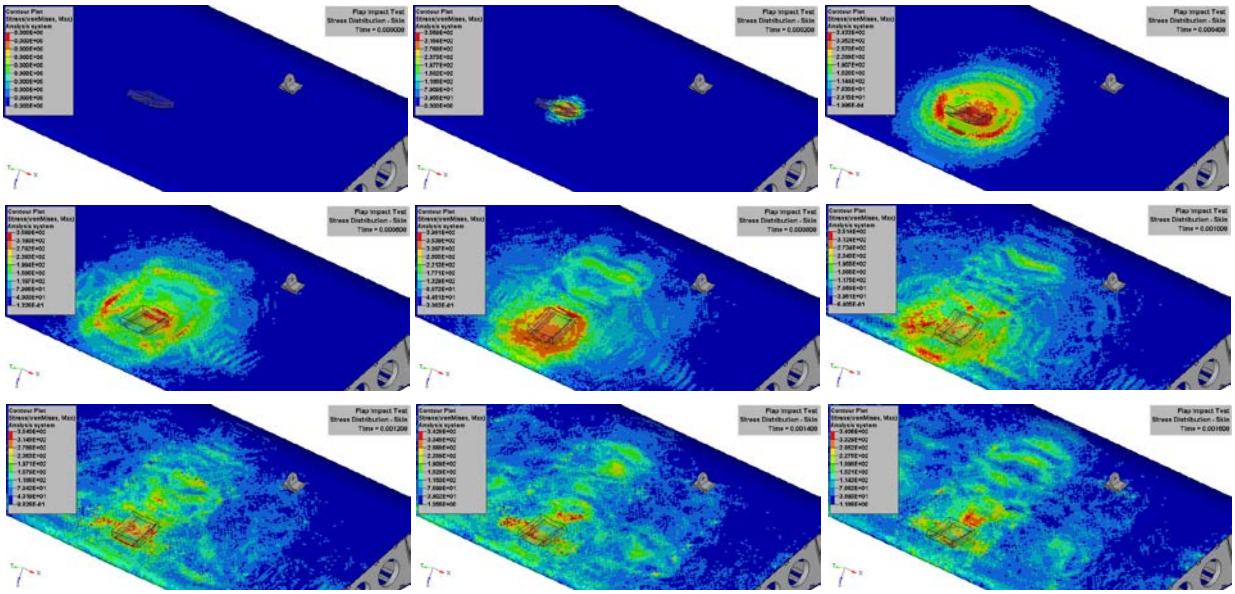

Figure 5.34 Stress distributions on the skin impacted by tire debris with 94 m/s.

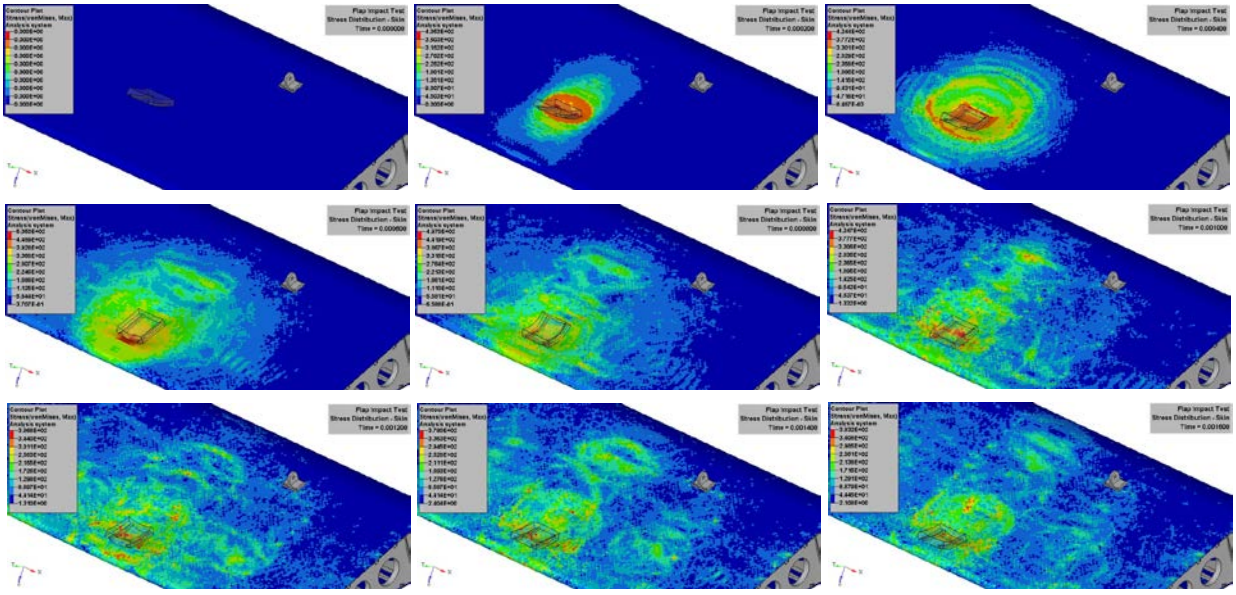

Figure 5.35 Stress distributions on the skin impacted by the tire debris with 135 m/s.

5.5.3. Inboard Flap at 37^0 Angle of Attack

In this case, validated tire debris model is impacted onto the inboard flap which is oriented at 37^0 to the ground plane with velocities of 94 m/s and 135 m/s.

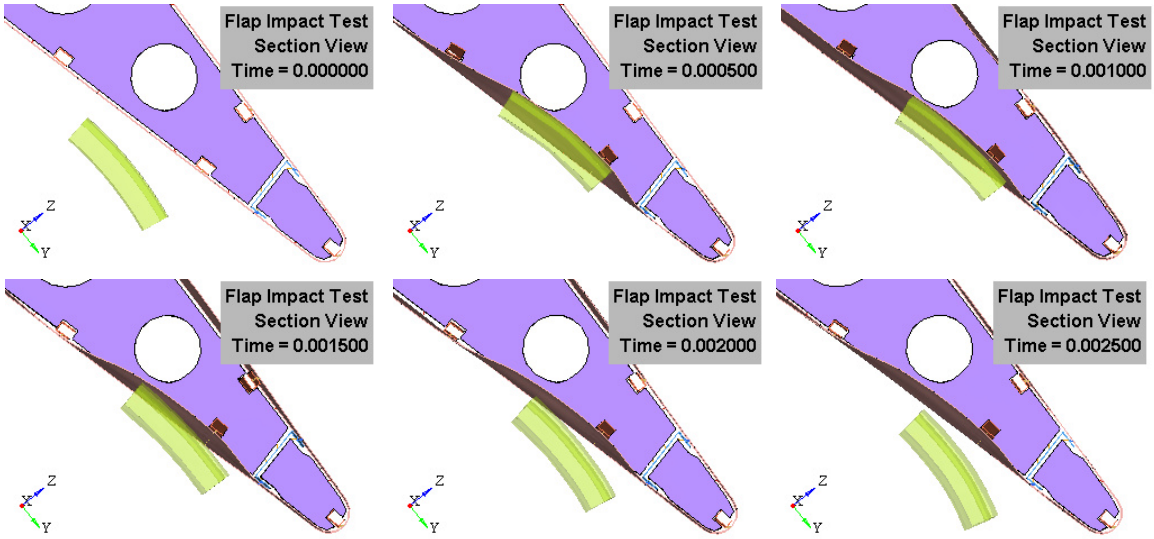

Figure 5.36 Time frames of the impact with a velocity of 94 m/s.

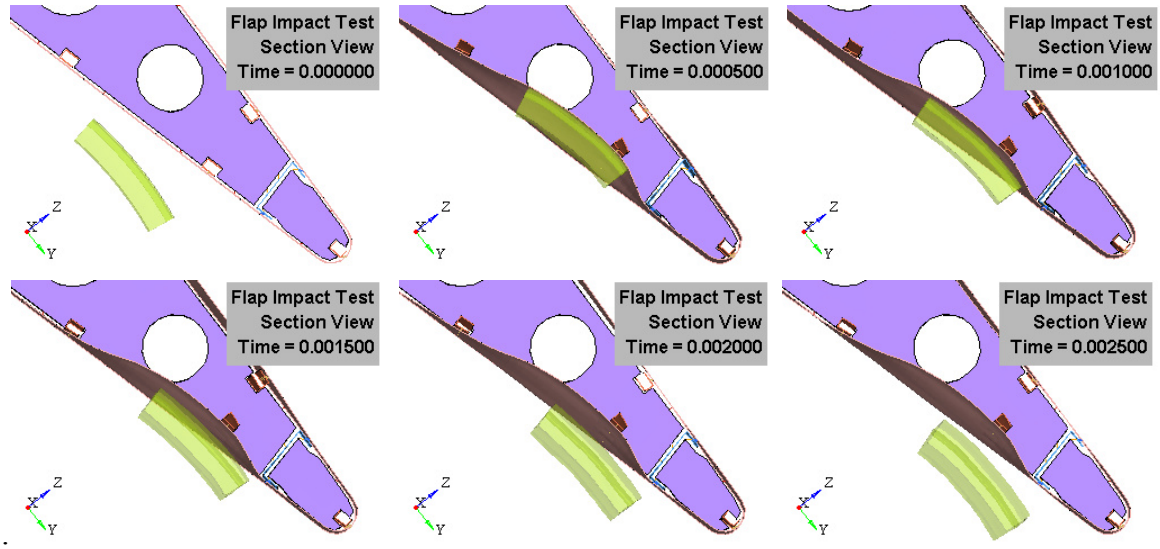

Figure 5.37 Time frames of the impact with a velocity of 135 m/s.

Time frames for the impact of tire debris on to the flap with velocity of 94 m/s are shown in the figure 5.36 and time frames for the impact of tire debris on to the flap with velocity of 135 m/s are shown in the figure 5.37. More deformation can be observed in the stringer and skin located in the impact zone when impacted by tire debris at 135 m/s.

Effective plastic strain for the skin is calculated after the impact with tire debris for the two velocity cases as shown in the figure 5.38. Higher plastic strain of 0.1087 is observed in the skin impacted by tire debris with a velocity of 135 m/s. More percentage of plastic strain is observed in the skin impacted with high velocity.

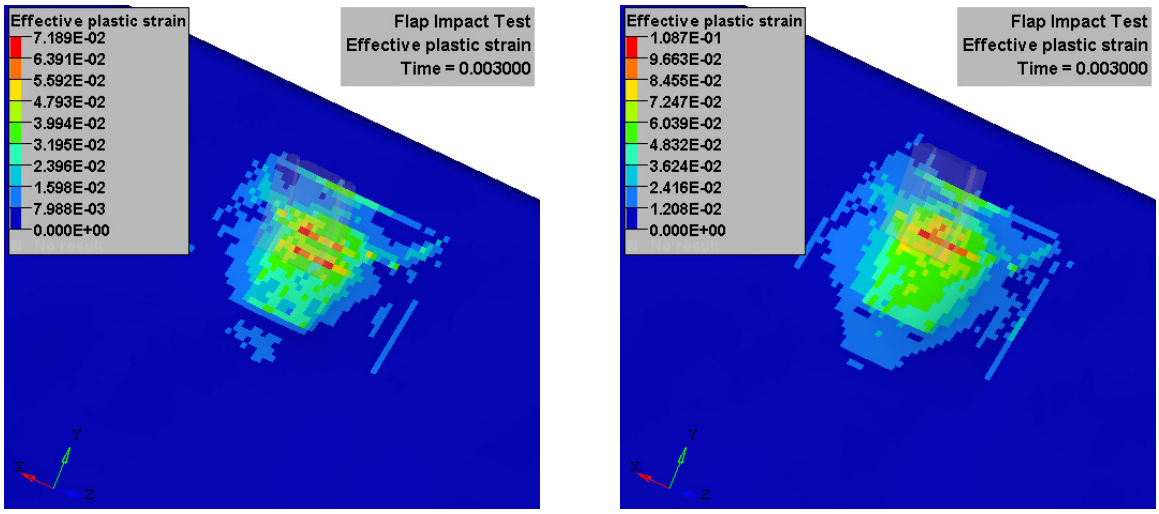

Figure 5.38 Effective plastic strains in the skin impacted by tire debris with 94 m/s & 135 m/s.

Stress distributions on the skin impacted by tire debris with 94 m/s and 135 m/s are shown in the figure 5.39 and 5.40 respectively. High regime of stress distribution is observed on the skin during impact time of 0.8 milliseconds. In the case of tire debris impacting with 94 m/s, stress of 423 MPa is calculated on the skin. But in the case of tire debris impacting with 135 m/s, stress of 467 MPa is calculated on the skin.

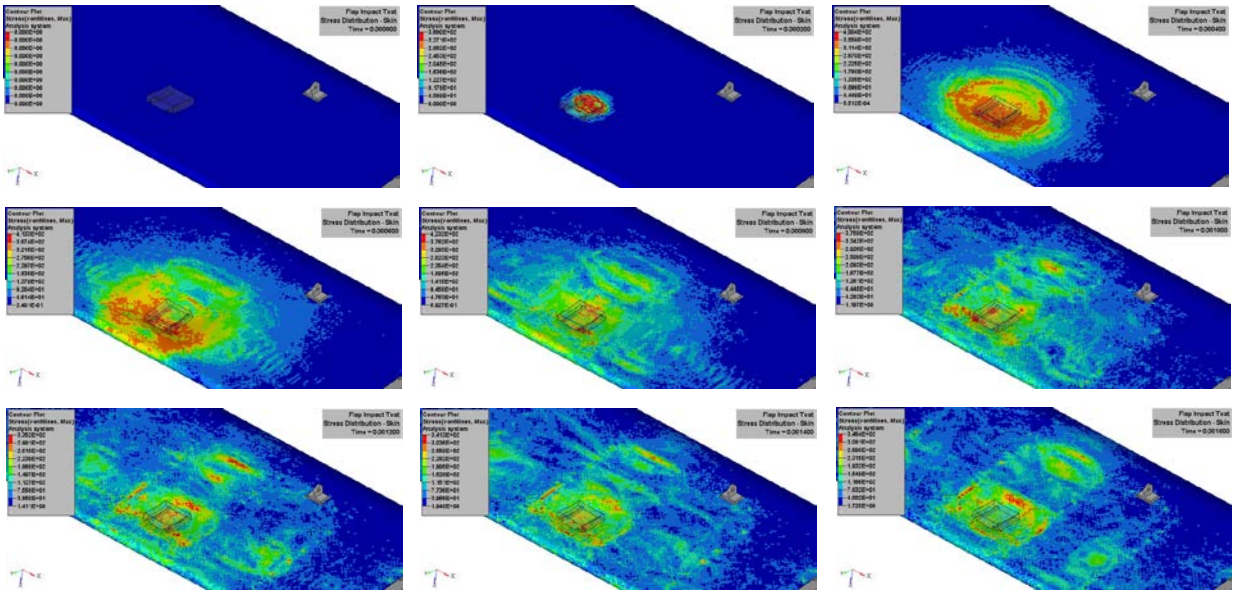

Figure 5.39 Stress distributions on the skin impacted by tire debris with 94 m/s.

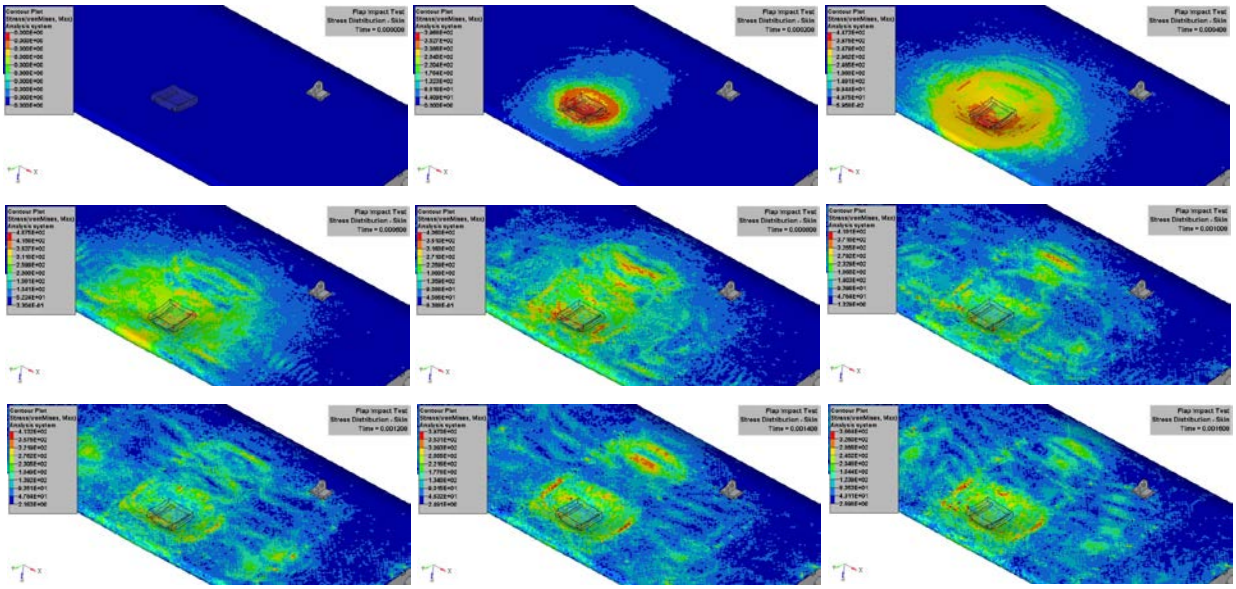

Figure 5.40 Stress distributions on the skin impacted by the tire debris with 135 m/s.

5.5.4. Energy Results for Flap Impact Analysis

Kinetic energies and internal energies are calculated for all the cases of flap impact analysis at location 2. Ratio of total energy of the system to initial energy of the system is equal to 1 as shown in the figure 5.41.

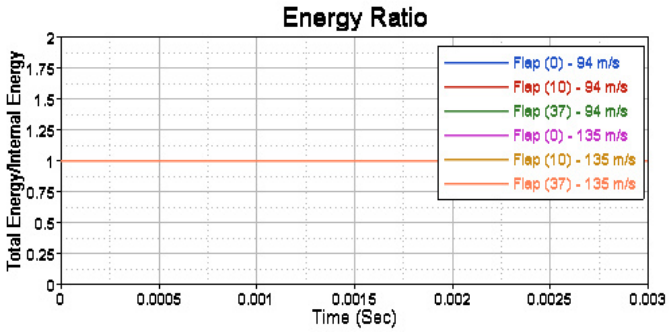

Figure 5.41 Energy Ratio of the system.

After the tire debris is impacted at location 2, its kinetic energy is transferred onto the skin and stringers located at impact location. Kinetic energy is lost in the tire debris model after it impacts the inboard flap assembly. Kinetic energy in the tire debris for all the six impact cases can be seen in figure 5.42. It can be noted that when tire debris impacts flap oriented at 37^0 with both velocities of 94 m/s and 135 m/s, they have the same amount of kinetic energy loss.

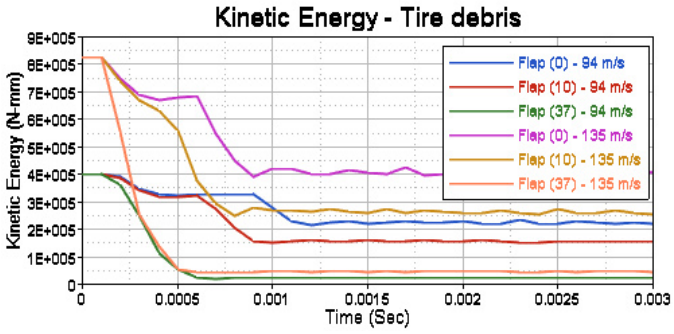

Figure 5.42 Kinetic Energy in tire debris model.

Internal energy gained in structural parts of rear spar and skin is show in figure 5.43 and figure 5.44 respectively. After tire debris impacts rear spar, there is gradual increase in internal energy for flap oriented at 0^0. More internal energy can be observed in the skin when tire debris impacts the flap oriented at 0^0 with a velocity of 135 m/s.

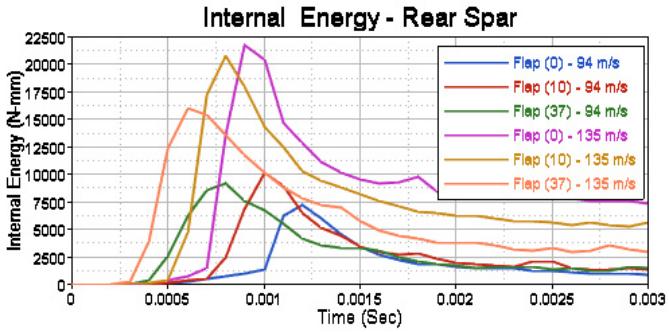

Figure 5.43 Internal Energy in the rear spar.

Internal energy in the skin increases gradually for the flap at 0^0 and 10^0, but for the flap at 37^0 there is abrupt increase in energy for tire debris impacting with a velocity of 94 m/s. A huge difference in internal energies for the skin can be observed when the tire debris impacts at 94 m/s and 135 m/s.

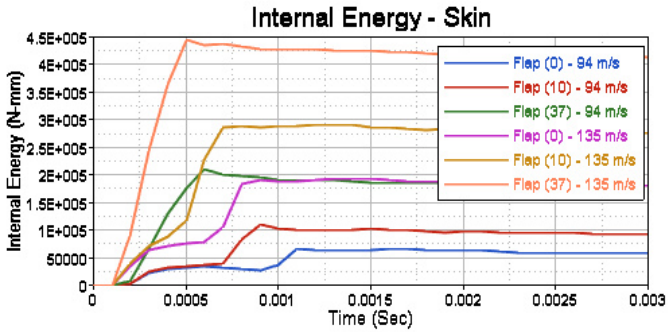

Figure 5.44 Internal Energy in the skin.

Results for structural integrity of the parts are tabulated for all 12 different cases for the parametric studies below. Case 1, 2 and 3 are tire debris impacting inboard flap at location 1 oriented at 0^0, 10^0 and 37^0 respectively at 94 m/s. Case 4, 5 and 6 are tire debris impacting inboard flap at location 1 oriented at 0^0, 10^0 and 37^0 respectively at 135 m/s.

TABLE 5.2

TABULATED RESULTS FOR INBOARD FLAP ANALYSIS AT LOCATION 1

Impact location 1	**Units**	**Case 1**	**Case 2**	**Case 3**	**Case 4**	**Case 5**	**Case 6**
Velocity – Tire debris	**m/s**	**94**	**94**	**94**	**135**	**135**	**135**
Flap Orientation	**deg**	**0**	**10**	**37**	**0**	**10**	**37**
Displacement on Skin	**mm**	11.9	13.1	11.6	17.0	17.5	15.3
Axial Force in Fastener	**N**	1696.0	1379.0	1395.0	1468.0	1624.0	2216.0
Shear Force in Fastener	**N**	1006.0	704.0	737.0	756.0	608.0	474.0
Plastic Strain - Skin	**-**	0.079	0.067	0.058	0.13	0.096	0.090
Stress - Skin	**MPa**	435.0	400.0	399.0	493.0	459.0	436.0
KE – Tire Debris	**N-m**	96.4	20.0	16.8	164.0	49.5	37.4
IE – Skin	**N-m**	162.0	194.0	185.0	397.0	418.0	398.0
IE - Stringer	**N-m**	26.0	44.0	56.0	70.0	93.0	108.0

Results include displacement of skin in Z direction in the impact location, effective plastic strain in the skin. Axial and shear forces in fasteners at impact location, maximum stress on

skin, kinetic energy for the tire debris after the impact, maximum internal energies in skin, stringers and rear spar. Case 7, 8 and 9 are tire debris impacting inboard flap at location 2 oriented at 0^0, 10^0 and 37^0 respectively at 94 m/s. Case 10, 11 and 12 are tire debris impacting inboard flap at location 2 oriented at 0^0, 10^0 and 37^0 respectively at 135 m/s. Results for impact location 1 are tabulated in table 5.2. Results for impact location 2 are tabulated in table 5.3.

TABLE 5.3

TABULATED RESULTS FOR INBOARD FLAP ANALYSIS AT LOCATION 2

Impact location 1	**Units**	**Case 7**	**Case 8**	**Case 9**	**Case 10**	**Case 11**	**Case 12**
Velocity – Tire debris	**m/s**	**94**	**94**	**94**	**135**	**135**	**135**
Flap Orientation	**deg**	**0**	**10**	**37**	**0**	**10**	**37**
Displacement on Skin	**mm**	5.2	8.9	12.1	8.2	12.0	17.1
Axial Force in Fastener	**N**	1041.0	1344.0	1348.0	777.0	1816.0	872.0
Shear Force in Fastener	**N**	554.0	704.0	1089.0	346.0	608.0	554.0
Plastic Strain - Skin	**-**	0.051	0.055	0.071	0.143	0.146	0.108
Stress - Skin	**MPa**	388.0	398.0	423.0	458.0	505.0	467.0
KE – Tire Debris	**N-m**	216.0	149.0	19.0	389.0	250.0	44.0
IE – Skin	**N-m**	66.0	109.0	210.0	194.0	291.0	445.0
IE - Stringer	**N-m**	7.0	10.0	9.0	21.0	20.0	16.0

Case 7, 8 and 9 are tire debris impacting inboard flap at location 2 oriented at 0^0, 10^0 and 37^0

respectively at 94 m/s. Case 10, 11 and 12 are tire debris impacting inboard flap at location 2 oriented at 0^0, 10^0 and 37^0 respectively at 135 m/s. Results for impact location 1 are tabulated in table 5.2. Results for impact location 2 are tabulated in table 5.3.

In the case of impact location 1, Maximum displacement of 17.5 mm was observed for case 5. Axial force in fastener was higher for case 6 with 2216 N. We can observe failure in this fastener as it has crossed the threshold value of 1800 N. Shear force of 474 N was observed for the same case which was lower than other cases, as the tire debris impacts almost perpendicularly onto this location. We can observe higher percentage of plastic strain in the case of 1 and 4 as the tire debris impacts onto the skin and slides along its path. Kinetic energy in the tire debris was reduced to 16.8 and 37.4 N-mm in case 3 and 6 respectively as the tire debris was impacted perpendicular to the flap. Gain in internal energy on the skin was observed to be 194 and 410 N-mm for case 2 and case 5 respectively.

In the case of impact location 2, Maximum displacement of 17.1 mm was observed for case 12. Axial force in fastener was higher for case 11 with 1816 N. We can observe failure in this fastener as it has crossed the threshold value of 1800 N. Shear force of 346 N was observed for case 10 which was lower than other cases. We can observe higher percentage of plastic strain in the case 11 as the tire debris impacts onto the skin and slides along its path. Kinetic energy in the tire debris was reduced to 19 and 44 N-mm in case 9 and 12 respectively as the tire debris was impacted perpendicular to the flap. Gain in internal energy on the skin was observed to be 210 and 445 N-mm for case 9 and case 12 respectively. We can conclude that over all behavior of the tire debris impacting inboard flap resulted in less damage to the aircraft structural components. It was observed that there was no penetration of tire debris into skin.

CHAPTER 6

CONCLUSIONS AND RECOMMENDATIONS

6.1 Conclusions

The objective of this research was to develop a methodology to certify an aircraft for tire debris impact by numerical analysis method. European Aviation Safety Agency's notice of proposed amendments [10] demonstrated that the structural components and systems which were essential to the safe operation of aircraft should be protected from the damaging effects of tire debris. The structure must withstand impact energy to prevent a catastrophic failure situation. In order to certify the aircraft's structural components against tire debris impact, Small tire debris model had to be used specified by EASA's certification standards. Small debris model is defined to have 1% of the total tire mass with distribution of impact load over an area which is 1.5 times the area of the tire tread.

This study provided a methodology to certify an aircraft for tire debris impact by numerical analysis method. Nonlinear finite element models of the tire debris and structural components were developed. Experimental data from the tire fragment impact test on to the aluminum plate [23] was compared with the simulation data to validate the tire tread model. All the required models were designed in Catia V5 R21. Finite element mesh was created using Altair Hypermesh 12.0. Material cards were created in LS Prepost 4.0. Pre analysis was simulated in LS Dyna by inputting experimental material data for rubber model and calculating strain energy constants. Post analysis was performed with revised material properties for rubber model. Strains at impact locations were calculated from strain gauges located on aluminum plate from experimental test and were compared with numerical simulation data to validate the

tire debris model. The comparison shows a reasonable correlation between experimental test results and numerical simulation results.

European Aviation Safety Agency and Federal Aviation Administration standards define that the tire debris can be impacted to any structural part which lies in the zone of vulnerability. Aircraft inboard flap is one of the major structural parts which are located in this zone of vulnerability. Parametric study was conducted by impacting the tire debris model onto the aircraft inboard flap. CAD for the inboard flap [4, 5] and tire debris model [26] were created using Catia V5 R21. Finite element mesh and fastener connections were created using Altair Hypermesh 12.0. Material properties and boundary conditions were assigned for the components using LS-Prepost 4.2. Two impact locations were considered on the flap where tire debris will be impacted with velocity of 94 m/s and 135 m/s on each location. Deformations of the structure are studied at these two locations by impacting the tire debris onto the flap oriented at 0^0, 10^0& 37^0 to the ground horizontal. Energy analysis was performed to determine the pass fail criteria of the structure. Fastener forces were considered for failure analysis.

Comparison of numerical simulation and experimental simulation shows a reasonable correlation for tire debris model. No penetration of tire debris into structural components was observed for the parametric study. Maximum displacement in skin was observed in the case of tire debris impacting onto flap oriented at 37^0 with higher velocity. Failure in fasteners at impact location was observed when the tire debris impacted onto flap oriented at 37^0 with higher velocity. There was no much difference in distribution of stress observed on the skin for all the impact cases. Overall variation of stress is less than 50MPa for the case of tire debris impacting flap oriented at different angles with same velocity. High percentage of plastic strain was observed in the case of flap oriented at 10^0 impacting at location 1 and 2 with higher

velocity.

This methodology can provide design engineers the effects of tire debris impact on a structural component and also help to change initial design requirements for structural components. This methodology can be used as “Certification by Analysis” and it provides cost saving alternative to experimental tests. There can be an efficient way to certify the aircraft structural components by finite element analysis tools. When compared to experimental tests, numerical simulation can be repeated number of times and also plays an important role during design optimization of the structural components. This methodology can also be utilized for the prediction of catastrophic scenarios.

6.2 Recommendations

From conclusions, deformations in the structural components can be studied to determine the failure criteria. Energy analysis also helps in determining the behavior of the structural components. Static and dynamic coefficient of friction values assigned to the *CONTACT cards in LS-Dyna will have impact on the results from simulations.

For the future work, variation in the simulation results can be observed by varying the coefficient of friction values from 0.1 to 0.9. The effect of drag on the tire debris before the impact will have a variation on the velocity and energy of the system. Thermal and structural interactions can be considered to study in-depth failure effects of the structural components.

For future work, hyperelastic behavior of rubber model can be utilized with more efficient way by assigning more strain energy constants for Mooney Rivlin material model. Additional study can be done on different tire debris modelling methods.

REFERENCES

REFERENCES

[1] Accident on 25 July 2000 at La Patte d'Oie in Gonesse (95) to the Concorde registered F-BTSC operated by Air France, BEA Accident Report F-SC000725A, BEA, France, January, 2002.

[2] CJI N998AM Occurrence Investigation Report, ASC Accident Report AOR-07-01-001, Aviation Safety Council, Taipei, Taiwan, January 25, 2007.

[3] NTSB Accident Report, Boeing 747-122 Reg-N4714U, National Transportation Safety Board, DCA85AA003, November, 1984.

[4] Bruhn, E.F., *Analysis and Design of Flight Vehicle Structures*, Austin: Jacobs, 1973.

[5] Michael, C. Niu., *Airframe Stress Analysis and Sizing*, Wanchai: Conmilit, 1997.

[6] Schoensleben, S. P., — *Integrated Trailing Edge Flap Track Mechanism for Commercial Aircraft*, ETH, Eidgenössische Technische Hochschule Zürich, Center of Structure Technologies, 2006.

[7] Federal Aviation Administration Advisory Circular 25.963-1, Fuel Tank Access Covers, July 29, 1992.

[8] Federal Aviation Administration Advisory Circular 25.1309-1A, System Design and Analysis, June 22, 1988.

[9] Federal Aviation Administration Advisory Circular 25.729-1, Transport Airplane Landing Gear Retracting Mechanism, December 28, 2011.

[10] European Aviation Safety Agency AMC 25.734, Protection against Wheel and Tyre Failures, January 18, 2013.

[11] Flight Safety Foundation, Pilot Guide to Takeoff Safety, 2012.

[12] LS-Dyna Keyword User's Manual, Volume I & II, Livermore Software Technology Corporation, May 26, 2014.

[13] Ryabov, A., Romanov, V., and Kukanov, S. S., Numerical Simulation of Consequences of Passenger Aircraft Tyre Damage, 8th European LS-Dyna Users Conference, Strasbourg, May, 2011.

[14] Reid, J. D., Boesch, D. A., and Bielenberg, R. W., Detailed Tire Modeling for Crash Applications, International Journal of Crashworthiness, Vol.12, Issue.5, pp. 521–529, October, 2007.

[15] Barbani, D., Pierini, M., and Baldanzini, N., FE Modelling of a Motorcycle Tyre for Full-scale Crash Simulations, *International Journal of Crashworthiness*, Vol.17, Issue.3, pp.309–318, February, 2012.

[16] Orengo, F., Ray, M. H., and Plaxico, C. A., Modelling Tire Blow-out in Roadside Hardware Simulations using LS-Dyna, Proceedings of the ASME International Mechanical Engineering Congress, Washington, DC, 2003.

[17] Konde, A. K., Rosu, I., and Lebon, F., Thermomechanical Couplings in Aircraft Tire Rolling/Sliding Modeling, Advance Materials Research, Vol.274, pp.81-90, 2011.

[18] Shang, R., Altenhof, W., and Li, N., Wheel Impact Performance with Consideration of Material Inhomogeneity and a simplified approach for modeling, International Journal of Crashworthiness, Vol.10, Issue.2, pp.137–150, 2005.

[19] Guo, H., Bastien, C., and Blundell, M. V., A Detailed Aircraft Tyre Finite Element Model for Hard Landing Safety Assessment, 9th European LS-Dyna Users Conference, Manchester, 2013.

[20] Yang, X., Behroozi, M., and Olatunbosun, O. A., A Neural Network Approach to Predicting Car Tyre Micro-Scale and Macro-Scale Behaviour, Journal of Intelligent Learning Systems and Applications, Vol.6, pp.11-20, 2014.

[21] Birch, R. S., Bergler, C., and Mines, R. A. W., Post-test Simulation of Airliner Wing Access Panel Subject to Tyre Debris Impact, 5th European LS-Dyna Users Conference, Birmingham, 2005.

[22] Lyle, K., Fasanella, E., and Gabrys, J., Application Of Non-Deterministic Methods To Assess Modelling Uncertainties For Reinforced Carbon-Carbon Debris Impacts, 5th International LS-Dyna Users Conference, Detroit, 2004.

[23] Mines, R. A. W., Karagiozova, D., Impact of Aircraft Rubber Tyre Fragments on Aluminum Alloy Plates: I-Experimental, *International Journal of Impacting Engineering*, Vol.34, Issue.4, pp.627–646, 2007.

[24] Mines, R. A. W., Karagiozova, D., Impact of Aircraft Rubber Tyre Fragments on Aluminum Alloy Plates: II-Numerical Simulations using LS-Dyna, *International Journal of Impacting Engineering*, Vol.34, Issue.4, pp.647–667, 2007.

[25] Rigby, R. H., Khalil, M., and Fouinneteau, M. R. C., Tire Debris Impact Modeling on a Composite Wing Structure, *Simulia Community Conference*, 2013.

[26] Engineering Data Book – Michelin Aircraft Tyre, Clermont-Ferrand Cedex 9 – France, URL: http://www.airmichelin.com/uploadedFiles/MichelinAirDev/StandardContent/Resource/databook.pdf. [Cited May, 2014].

[27] Learjet Business Class Jet., Bombardier Aerospace., 2015, – Specification Drawings, URL: http://businessaircraft.bombardier.com/en/aircraft/learjet/learjet85.html#nb_aircraft_2.

[28] United States, and Battelle Memorial Institute., 2008, MMPDS-04 Metallic Materials Properties Development and Standardization, Washington, D.C.: Federal Aviation Administration, URL: http://app.knovel.com/hotlink/toc/id:kpMMPDSM01/metallic-materials-properties.